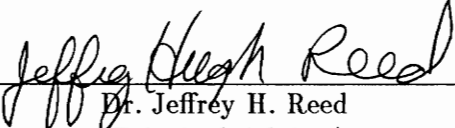# OPTIMUM LINEAR SINGLE USER DETECTION IN DIRECT-SEQUENCE SPREAD-SPECTRUM MULTIPLE ACCESS SYSTEMS

by

Volker Aue

Thesis submitted to the Faculty of the

Virginia Polytechnic Institute and State University

in partial fulfillment of the requirements for the degree of
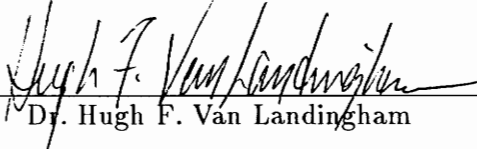
MASTER OF SCIENCE

in

Electrical Engineering

Approved:

Dr. Jeffrey H. Reed
(Principal Adviser)

Dr. Brian D. Woerner

Dr. Hugh F. Van Landingham

Blacksburg, Virginia

Optimum Linear Single User Detection in Direct-Sequence Spread-Spectrum Multiple Access Systems

by

Volker Aue

Committee Chairman: Dr. Jeffrey H. Reed

Electrical Engineering

Abstract

After Qualcomm's proposal of the IS-95 standard, *code-division multiple access* (CDMA) gained popularity as an alternative multiple-access scheme in cellular and *personal communication systems* (PCS). Besides the advantage of allowing asynchronous operation of the users, CDMA *direct-sequence spread spectrum* (DS-SS) offers resistance to frequency selective fading and graceful degradation of the performance as the number of users increases.

Orthogonality of the signals in time-division multiple access and frequency-division multiple access is inherent from the nature of the multiple access scheme. In a CDMA system, orthogonality of the signals is not guaranteed in general. Consequently, the performance of conventional correlation receivers suffers.

Sub-optimum receivers which use knowledge of the interfering signals have been investigated by other researchers. These receivers attempt to cancel the multi-user interference by despreading the interfering users. Hence, these receivers require knowledge about all the spreading codes, amplitude levels, and signal timing, and are, in general, computationally intensive.

In this thesis, a technique is presented for which a high degree of interference rejection can be obtained without the necessity of despreading each user. It is shown that exploiting spectral correlation can help mitigate the effects of the multiple-access interference. If *code-on-pulse* DS-SS modulation is used, a cyclic form of the Wiener filter provides substantial improvements in performance in terms of bit error rate and user capacity. Furthermore, it is shown, that a special error-criterion should be used to adapt the weights of the filter.

The computational complexity of the receiver is equivalent to that of conventional equalizers.

Preface

The research presented in this thesis was originally motivated by investigating how a *radial basis function* (RBF) network [1] could be used to help reject interference in a multiple access system. The multiple access interference in a CDMA system is often non-Gaussian. Under this condition, a non-linear optimal filter can provide better performance than a linear filter. Also, to keep the design simple and computationally efficient, a single user detector was proposed.

The basic idea was to apply an RBF neural network at the output of a tapped delay line with a length of the bit-duration T_b. The outputs of the shift-registers composing the delay line form the input space of the RBF receiver. By using bit-repetitive spreading codes, demodulation and despreading a desired user is viewed by the RBF neural network as a pattern recognition problem. This can be understood as follows: In the noiseless case, a bit multiplied by the spreading code corresponds to a certain pattern. For BPSK signaling, each user produces two patterns, one pattern corresponding to a 'one,' and another pattern corresponding to a 'zero.' If the outputs of the tapped delay line hold an entire bit and are presented to the neural network at the bit rate, the neural network views the process of demodulation as a pattern recognition problem of a pattern in an N_1-dimensional space, where N_1 is the number of taps. By sending a *training sequence* first, the RBF network learns the decision rule.

Figure 1 depicts the principal structure of the RBF receiver. Each RBF is connected to all samples within the delay line. For the neural network, the outputs of the delay line form the input vector $\mathbf{x}$. At the bit rate, the RBFs $\Phi_j(||\mathbf{x} - \mathbf{c}_j||), 1 \leq j \leq N_2$, are calculated. Then, the function values are scaled by some factors $w_j, 1 \leq j \leq N_2$, and summed to form the network output. Also, a threshold value $\Theta = w_0$ is added. The network output is one dimensional, since the network has only to decide whether a 'one' or a 'zero' is transmitted. A hard-limiting function

$$f_{\mathrm{HL}}(y) = \begin{cases} 1, & y \geq 0, \\ -1, & y < 0, \end{cases} \tag{1}$$
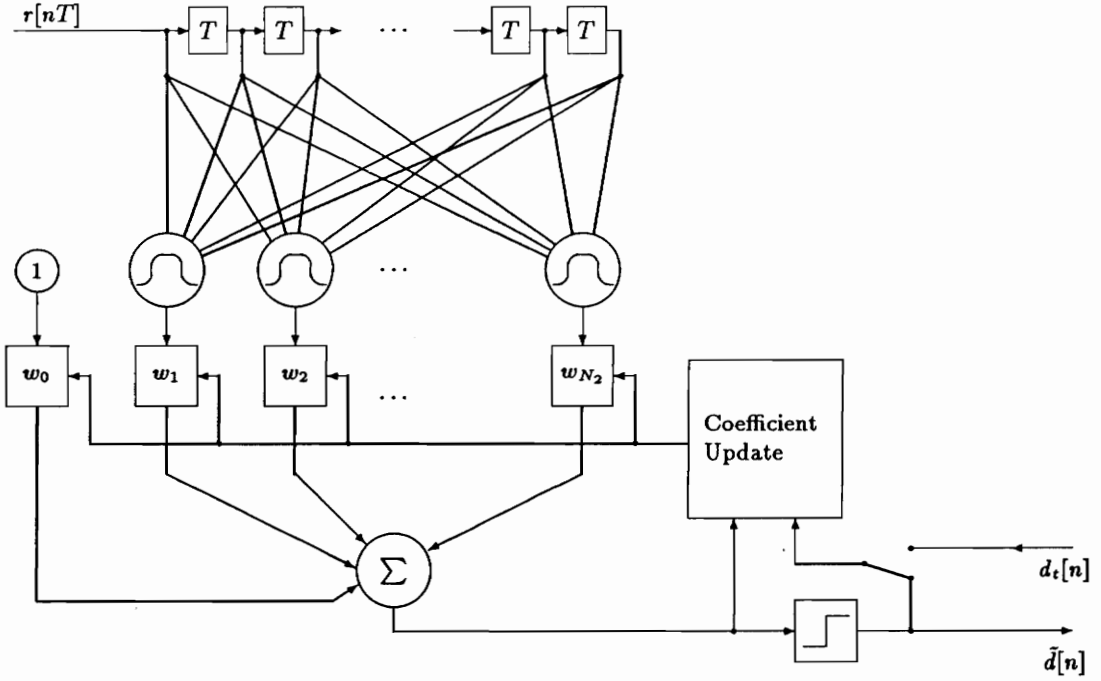
Figure 1: The radial basis function receiver.

decides that a 'one' is transmitted when the output of the RBF neural network is positive and a 'zero' is transmitted when the network output is negative.

A coefficient update algorithm compares the network output with a desired output and updates the weights to minimize the error in a *least-squares* sense. In *training mode*, the comparison takes place between the network output and the known training symbols. After training is completed, the coefficient update is switched to *decision-directed mode* and the output of the neural network is compared to the output of the hard-limiter.

For multiple users, the number of possible patterns, n, grows exponentially with the number of users, K, and it can be shown that

$$n = 2^{2K-1}. \tag{2}$$

Simulations show that despite the exponential growth of possible patterns, the RBF neural network is able to establish a decision boundary which allows significant performance gains over conventional correlation receivers.

However, it turned out that this decision boundary is converging towards a linear decision boundary. Thus, the non-linear RBFs can be taken out from the design and a less computational intensive linear receiver can be proposed.

Acknowledgements

I would like to express my gratitude to Dr. J. H. Reed for his helpful insights, directions, and many useful comments during the work on this thesis and the preparation of this manuscript.

I wish to thank my parents for their encouragement and support in my studies throughout these years.

I am most indebted to Antje for her love and patience during my studies abroad.

Contents

List of Tables

List of Figures

Chapter 1

Introduction

In the past, spread-spectrum techniques were reserved for military applications. Spread-spectrum signals are resistant to jamming and their relatively low power spectral density reduces the probability of interception. In recent years, spread-spectrum techniques have gained importance for commercial applications. Though demodulation of spread-spectrum signals appears to be more difficult than demodulation for conventional modulation schemes, its selective addressing capability and ability for code-division multiple access as well as interference rejection make spread-spectrum modulation useful for the cellular industry.

1.1 Comparison Between TDMA, FDMA, and CDMA

In a multiple user system like a cellular telephone system, it is necessary to employ a multiple access scheme to guarantee separation among the users. The traditional multiple access schemes are *time-division multiple access* (TDMA) and *frequency-division multiple access* (FDMA). In FDMA systems, each user is assigned a different frequency band, hence, it is relatively easy to separate each user from a group of users. However, since the available channels are, in general, narrowband channels, FDMA systems suffer heavily from frequency selective fading. Also, FDMA suffers from capacity loss due to channel spacing which is necessary to guarantee channel separation for Doppler-shifts in the transmitted signals and oscillator imprecisions. In a TDMA system, each user is assigned a different time slot in which the user may transmit a package of data. All users share the same channel but use it at different times. Since the bit rate during package transmission is higher than for continuous transmission, the channel bandwidth is considerably higher than for a single channel for FDMA. Although TDMA seems to overcome many of the reasons for capacity

degradation in FDMA systems, time-displacement, *intersymbol-interference* (ISI) and co-channel interference degrade the capacity of a TDMA system.

Hybrid systems, like time-slotted frequency hopped multiple-access, employing variations of the FDMA and TDMA schemes, generally suffer from the same degradation as the pure FDMA or TDMA schemes.

Another multiple-access scheme is *code-division multiple access* (CDMA). In a CDMA system all users share the same channel at the same time. A user is distinguished from other users by using a different waveform. In a direct-sequence spread spectrum (DS-SS) system, the waveform generation is obtained by multiplying a narrowband signal by a sequence of symbols typically from the alphabet $\{-1, 1\}$. By correlating with the sequence assigned to an individual user, the user can be separated from a received signal composed of superposition of all signals.

In theory, for the *additive white Gaussian noise* (AWGN) channel, FDMA, TDMA and CDMA are equivalent with respect to bandwidth efficiency or user capacity [2]. In the mobile radio environment, however, CDMA has been shown to offer some advantages over FDMA and TDMA, since it can compensate for the effects of frequency-selective fading and time-delay spreads [2].

Besides the performance gained by using CDMA in a mobile channel, employing a CDMA scheme provides several more advantages:

- The performance of a CDMA system degrades gracefully with increasing number of users.

- Asynchronous operation is possible.

- Bandwidth expansion due to Doppler-shifts is less significant compared to FDMA.

- The capacity loss due to multipath delays in the mobile channel is less than in TDMA systems.

On the other hand, CDMA also possesses some disadvantages:

- CDMA receivers and transmitters are more complex than those needed for TDMA or FDMA.

- Orthogonality between the users, which is an integral part of FDMA and TDMA schemes, is not generally owned by CDMA.

Due to recent advances in computational capabilities and digital signal processing, basic CDMA transmitters and receivers are now realizable at low costs. However, computational

2

complexity remains still an important factor especially when more sophisticated computationally intensive receivers are proposed, and since power consumption increases with the amount of computations. Especially at the mobile station, power consumption is a critical factor.

Non-orthogonal signaling results in *multiple-access interference* (MAI) limiting the capacity of the multiple-user system. A way to reduce the impact of MAI in a CDMA system is to control the power of each user. In the Qualcomm IS-95 proposal [3] long signature sequences with low cross-correlation properties are used to reduce CDMA interference. The receiver treats every user no differently than white Gaussian noise, thus every user contributes a fraction to the noise level. To minimize the impact of CDMA interference, power control is used to maintain consistent power levels among the users. Using Qualcomm's modulation scheme, the signals have almost no spectral correlation. However, if the spreading codes meet certain requirements, then spectral correlation in the *signal of interest* (SOI) and the interference can be exploited to help increase the performance of the receiver. This is discussed in Chapter 3. It is shown that substantial improvement can be gained by using bit repetitive signature sequences.

1.2   CDMA and Direct-Sequence Spread Spectrum

Obtaining a DS-SS signal can be viewed as multiplying a narrowband modulated signal $s_N(t)$ by a high-speed spreading sequence. The narrowband signal is spread over a larger bandwidth, and its *power spectral density* (PSD) is lowered by the *processing gain*. Though all different types of narrowband modulation schemes can be applied to DS-SS modulation, more simple modulation schemes like *binary phase shift keying* (BPSK) or *quadrature phase shift keying* (QPSK) are most commonly used.

The spreading sequence typically consists of symbols from a finite set. These symbols can be either real or complex values. For QPSK spread-spectrum, two different spreading sequences for the inphase and quadrature component of the narrowband signal are usually employed, and they are commonly chosen to be orthogonal to obtain maximum signal separation.

The generation of a BPSK DS-SS and its characteristics are discussed in the following section.

3

1.2.1 BPSK DS-SS Modulation and Waveform Description

BPSK modulation is accomplished by modulating the phase of a sinusoidal signal with the incoming data bit stream,

$$s_d(t) = A_c \cos[\omega_0 t + \Theta_d(t) + \varphi], \qquad (3)$$

where $\Theta_d(t)$ is either 0 or π depending on the data bits, ω_0 denotes the carrier frequency, A_c is the carrier magnitude, and φ is an arbitrary phase factor. It is well known, that

$$\cos(\pi + x) = -cos(x). \qquad (4)$$

Hence, Equation 3 can be rewritten as

$$s_d(t) = A_c d(t) \cos(\omega_0 t + \varphi). \qquad (5)$$

Thus, BPSK modulation can be achieved by multiplying a carrier with the data bit stream $d(t)$, where the data bits are symbols taken from the set $\{-1, 1\}$. The bandwidth of a BPSK signal depends on the data bit rate R_b. Its absolute bandwidth is infinite, whereas the 3-dB bandwidth of a BPSK signal is approximately $0.88R_b$. Its null-to-null bandwidth is $2R_b$.

A DS-SS system multiplies the modulated signal with a code sequence, $c(t)$, which is much faster than the bit rate. Therefore, the spread signal is

$$s_d(t) = A_c c(t) d(t) \cos(\omega_0 t + \varphi). \qquad (6)$$

$c(t)$ is the spreading sequence with values typically taken from the alphabet $\{-1, 1\}$.[1] The discrete symbols of the signature sequence are referred to as *chips*. Its duration T_c is called the *chip period*. If T_b denotes the data bit period, then the signal spectrum is spread by a factor of T_b/T_c called the *processing gain*. The amplitude spectrum of a BPSK signal with carrier frequency $f_c = 1049$ kHz and bit rate $R_b = 16.384$ kbit/s is depicted in Figure 2. Multiplying the BPSK signal with a processing gain of 32 (15 dB) reduces the amplitude of the BPSK signal and spreads it out over a bandwidth 32 times larger. The DS-SS signal is shown in Figure 3. Its null-to-null bandwidth is 1049 kHz. Figure 4 depicts a simplified block diagram of the DS-SS modulator.

1.2.2 Spreading Codes

Any chip sequence can be used for spreading a signal. For demodulating a DS-SS signal, the only constraint is that the spreading sequence is known at the receiver. However, not

---

[1] This constraint only holds for real spreading sequences. A complex spreading sequence might take values from the alphabet $\{-1, 1, -j, j\}$.

4
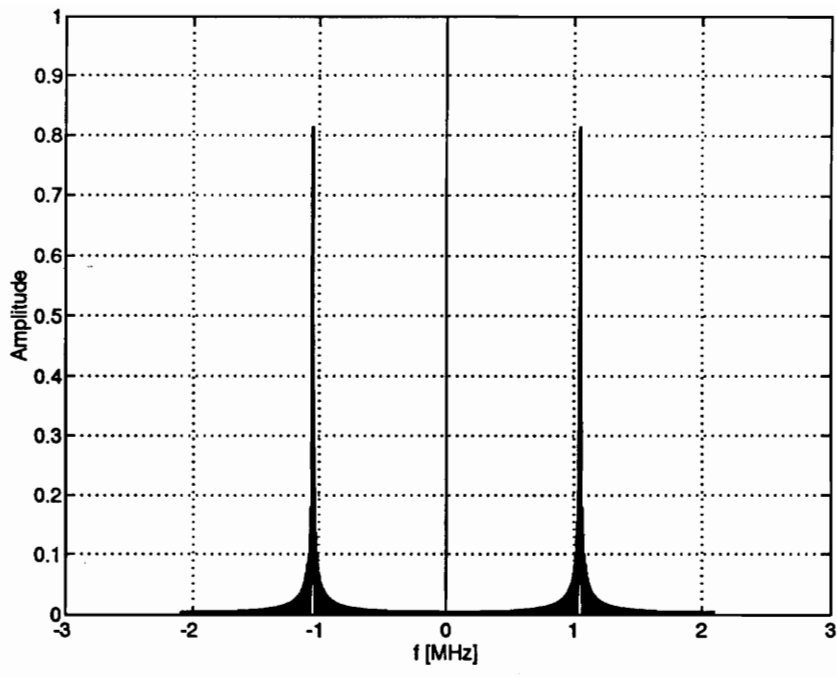
Figure 2: Spectrum of the BPSK signal.
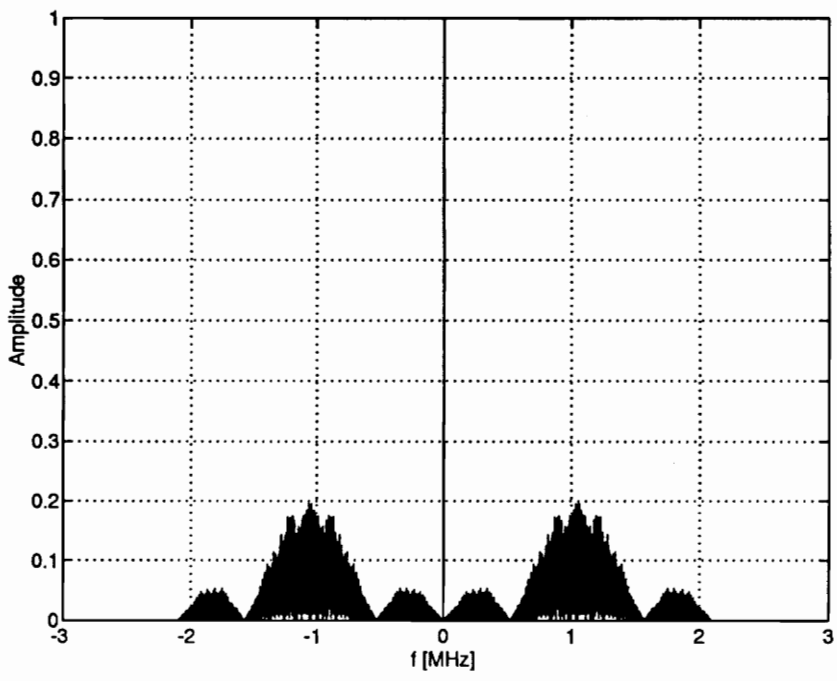
Figure 3: DS-SS signal.

5
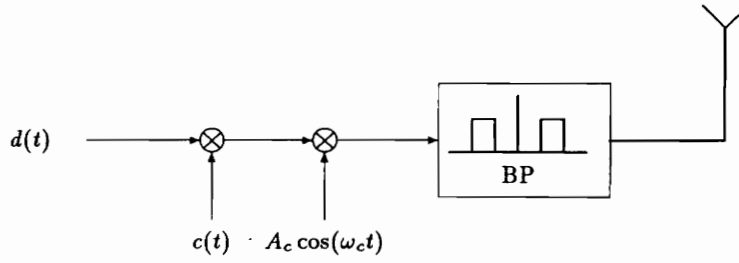
Figure 4: DS-SS modulator.

all sequences have the same spectral properties. In a CDMA system where other users occupy the same spectrum, low cross-correlations between different spreading sequences are desired. Finally, to be more resistant to multipath delays and to ease synchronization, a low autocorrelation for each code is desired. In some systems, the spreading sequences repeat with a certain period N. The spreading code $c(t)$ can be described by

$$c(t) = \sum_{m=-\infty}^{\infty} c_m q\left(\frac{t}{T_c} - m\right), \tag{7}$$

where c_m is taken from the alphabet $\{-1, 1\}$,[2] and $q(t)$ is the rectangular function

$$q(t) = \begin{cases} 1, & -\frac{1}{2} \leq t \leq \frac{1}{2}, \\ 0, & \text{otherwise.} \end{cases} \tag{8}$$

The autocorrelation $R_{cc}(\tau)$ of a code is then defined as

$$R_{cc}(\tau) = \frac{1}{T} \int_0^T c(t)c(t+\tau)\, dt, \tag{9}$$

and the cross-correlation between two sequences $c(t)$ and $c'(t)$ is given by

$$R_{cc'}(\tau) = \frac{1}{T} \int_0^T c'(t)c(t+\tau)\, dt. \tag{10}$$

Many different kinds of codes have been investigated by researchers. The most commonly known are *Gold* codes and *m*-sequences [4].

---

[2]See also Footnote 1.

Chapter 2

Current Techniques for CDMA Demodulation and Interference Rejection

2.1 Conventional Receiver

Referring to Section 1.2, a DS-SS signal results from multiplying a narrowband message signal with a spreading sequence with rates higher than the bit rate of the narrowband signal. The resultant signal occupies a higher bandwidth, but its PSD is lower than the original narrowband signal.

A formula expression for a BPSK DS-SS signal is given in Equation 6:

$$s_d(t) = A_c c(t) d(t) \cos(\omega_0 t + \varphi), \tag{11}$$

where $c(t)$ and $d(t)$ come from the binary alphabet $\{-1, 1\}$. If the spreading sequence is known at the receiver, a detected signal, $r(t)$, of the form $s_d(t) + n(t)$, where $n(t)$ is some noise or interference introduced by the communication channel, can be despread.

Before processing the received signal, in almost every receiver, the signal is shifted to a more convenient frequency, most commonly to *baseband*. First, the received signal is bandpass filtered to reject noise outside the signal bandwidth. Second, the signal is shifted to baseband by multiplying the signal by a frequency generated from a local oscillator and lowpass filtering. In discrete-time systems, a common technique is decimation. An *analytic* signal, i.e., a signal for which the Fourier transform only contains positive frequency components, can be obtained using the Hilbert transform [5]. The results presented in this thesis assume a baseband representation.
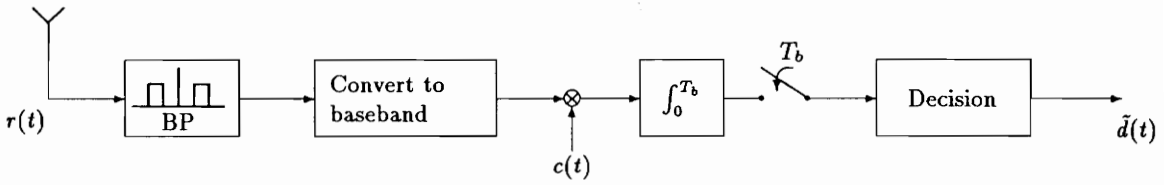
Figure 5: DS-SS demodulator using a correlator.
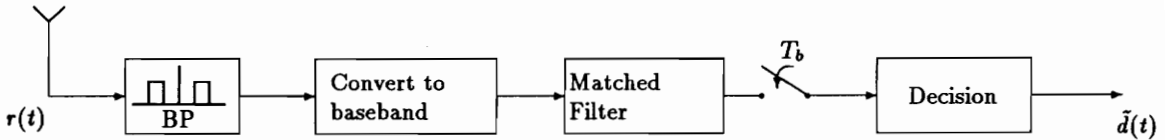
Figure 6: DS-SS demodulator using a matched filter.

2.1.1 Despreading by Correlation

Assuming that the receiver is synchronous with the received signal, despreading can be achieved by multiplying the received signal $r(t)$ with the conjugate complex code $c(t)$. Integrating the output of the multiplier and sampling the output at the bit rate yields an estimate $\tilde{d}(t)$ of the data bits $d(t)$. Figure 5 depicts the principal of the DS-SS demodulator described above. Note that the multiply and integrate functions are equivalent to a correlation operation.

Another implementation of a correlator is the *matched filter*. A matched filter is a linear filter that maximizes the SNR at its output. It can be shown that when only white Gaussian noise is added to the signal, the matched filter's frequency response $H(f)$ is the conjugated Fourier transform of the known signal $s(t)$ times a constant factor [6]. In a digital system, the matched filter is implemented as a linear transversal filter. Figure 6 shows the equivalent demodulator as in Figure 5 using a matched filter.

2.1.2 Performance of the Matched Filter

The matched filter can also be used to demodulate a DS-SS signal in a CDMA environment. This is because CDMA interference is approximately white and Gaussian. A close approximation of the performance of the matched filter for CDMA is given by Holtzman [7]. Assuming each user has uniform distributed phases, same amplitude levels, uniform distributed delays within one chip, and uses random codes, Holtzman found an expression

which gives an approximation of the probability of bit-error, P_e, depending on the number of users, K, the processing gain N, the energy per bit, E_b, and the noise power spectral density $\frac{N_0}{2}$:

$$P_e \approx \frac{2}{3}Q\left[\left(\frac{K-1}{3N} + \frac{N_0}{2E_b}\right)^{-0.5}\right]$$
$$+\frac{1}{6}Q\left[\left(\frac{(K-1)(N/3)+\sqrt{3}\sigma}{N^2} + \frac{N_0}{2E_b}\right)^{-0.5}\right]$$
$$+\frac{1}{6}Q\left[\left(\frac{(K-1)(N/3)-\sqrt{3}\sigma}{N^2} + \frac{N_0}{2E_b}\right)^{-0.5}\right], \tag{12}$$

with

$$\sigma^2 = (K-1)\left[N^2\frac{23}{360} + N\left(\frac{1}{20} + \frac{K-2}{36}\right) - \frac{1}{20} - \frac{K-2}{36}\right], \tag{13}$$

and $Q(\cdot)$ given by

$$Q(x) = \frac{1}{\sqrt{2\pi}}\int_x^\infty e^{-\frac{u^2}{2}}\, du. \tag{14}$$

The probability of error for the matched filter receiver according to Equation 12 is depicted in Figure 7 for $N = 7, 31, 63$. It can be seen that for a number of users greater than 30 percent of the processing gain N, the *bit-error rate* (BER) becomes intolerable.

Results similar to these derived by Holtzman can be found in [8]. This reference gives lower and upper bounds on the probability of bit error based on the same assumptions as in [7].

2.2 The Optimum Receiver

By treating interference introduced by multiple-access users as Gaussian noise, the matched filter does not exploit any knowledge of the other users. This short coming can be over-come by *multi-user detection*. Multi-user detection can be viewed as a bank of single-user detectors where a decision for a certain user is made using the outputs of all single-user detectors.

Assuming all users to be synchronous, finding an optimum symbol decision reduces to maximizing a quadratic function. For the asynchronous case the optimum receiver has been shown to have the form of a Viterbi forward dynamic programming algorithm [9] employed at the outputs of a bank of single user detectors.

Figure 8 illustrates the diagram of the optimum receiver. The received signal, $r(t)$, is passed through a bank of matched filters. The delays, τ_i, compensate for asynchronous
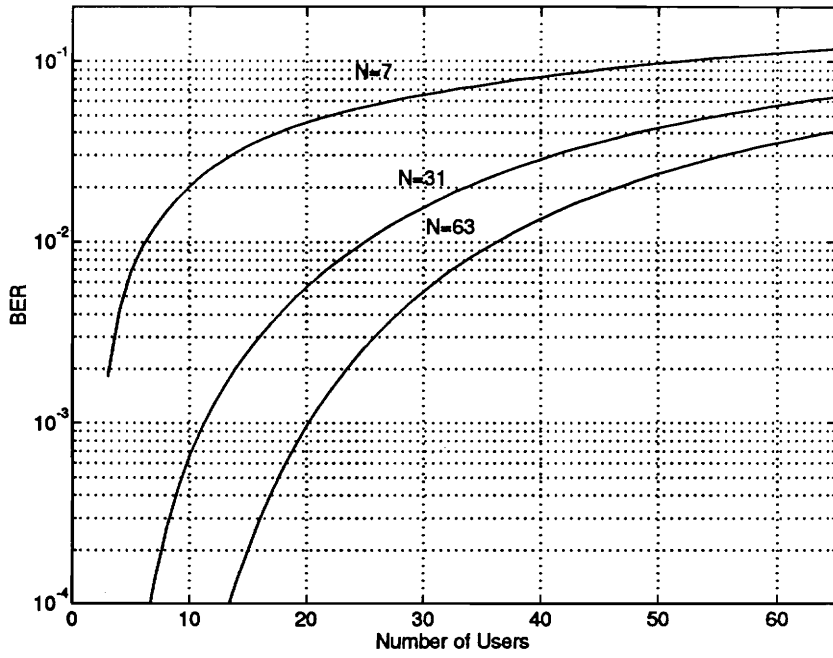
Figure 7: Performance of the matched filter.
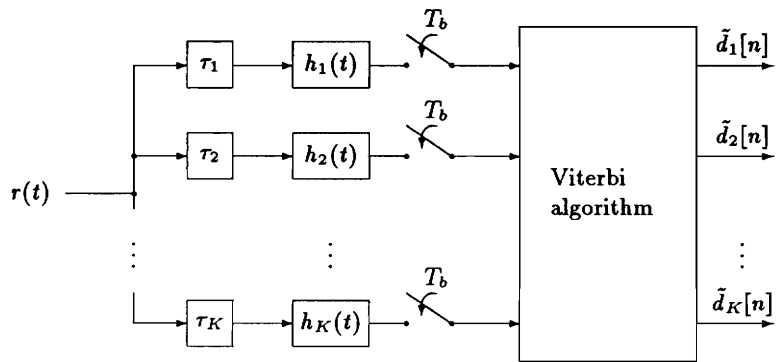
Figure 8: Diagram of the optimum receiver.

10
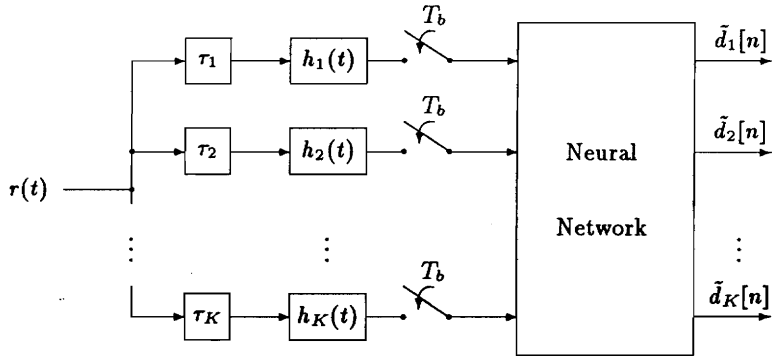
Figure 9: Diagram of the neural network receiver.

users. A Viterbi forward dynamic programming algorithm is applied at the outputs of the matched filters to make the optimum decision [10].

The complexity of the optimum receiver for both cases, the synchronous as well as the asynchronous case, has been shown by Verdú to increase nondeterministic polynomial-time hard (NP-hard) with the number of users, whereas its time-complexity increases linearly with the number of symbols sent by each user [11].

Due to the nondeterministic polynomial-time increase in complexity, the optimum receiver, as proposed by Verdú, can easily reach an infeasible number of computations. This is the case even for a relatively low number of users. If the number of users in a cellular system exceeds eight, the computational complexity exceeds practical limits. This is the case for almost all CDMA applications for cellular systems and PCS.

2.3   Neural Network CDMA Multi-User Detection

As mentioned in Section 2.2, the optimum receiver introduced by Verdú is infeasible for most practical applications. An attempt to reduce computational complexity is the receiver proposed by Behnaam Aazhang et. al. in [12]. In this approach, a multilayer perceptron neural network is applied to the outputs of a bank of matched filters. It is trained to approximate the Viterbi detector. Since the Viterbi detector yields Bayesian decision statistics for the CDMA problem, the neural network finds a suboptimum solution to multi-user detection. However, the computational effort is considerably less than for the Viterbi optimum receiver. The authors were able to demonstrate performance close to that of Verdú's receiver.

The neural network receiver is shown in Figure 9.

11
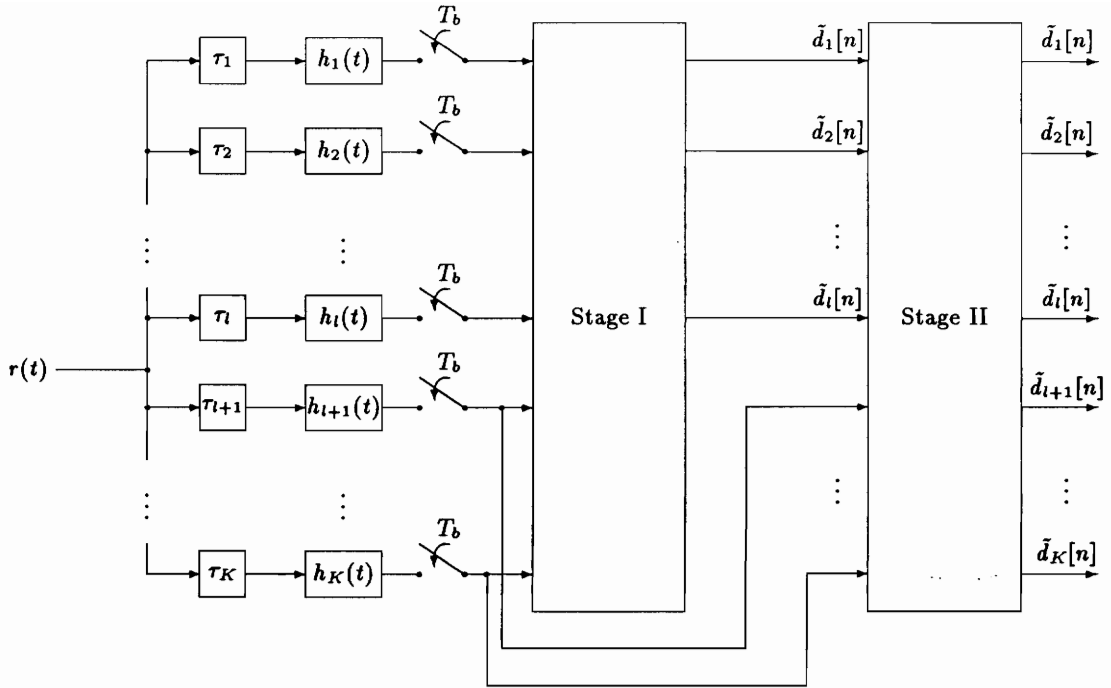
Figure 10: Multistage receiver.

2.4 Multistage Receivers for CDMA User Detection

Another approach used for multiuser detection are *multistage receivers* and are introduced in [13]. A multistage receiver demodulates the strongest users first; in a second step, after subtracting these users out of the received signal or the decision variables, it attempts to demodulate the remaining users. Thus, it is capable of rejecting performance degradation especially in the presence of widely different power levels among the users.

An example for a multistage receiver employing two stages is depicted in Figure 10. The first stage demodulates the first l users. The second stage uses the data estimates, $\tilde{d}[n], 1 \leq i \leq l$, to help detecting the remaining users. Note that multistage receivers with more than two stages exist.

The mobile channel and non-linearities introduced by amplifiers and antennas degrade the performance of multi-stage receivers. Since the mobile channel is subject to frequency-selective fading due to multipath delays, an accurate estimate of a multiuser component is almost impossible to obtain. Also, an accurate knowledge about all power levels in the system is necessary. Subtracting out an inaccurate estimate out of the received signal, leaves residual multiple access interference.

2.5 Summary

CDMA offers great potential for increasing the capacity of a multi-user system. However, the conventional correlation receiver is subject to the "near-far" problem and does not make use of the interference structure. As a result, the correlation receiver only supports a number of users approximately equal to 30 percent of the processing gain at a BER of 10^{-3}. Joint detection requires complete knowledge of the signals and its computational intensity makes the receiver very expensive, if not impractical.

In the subsequent chapters another effective way of MAI mitigation is discussed for which the computational effort is considerably less than for joint detection receivers, but which shows almost identical performance.

Chapter 3

Cyclostationarity in Direct-Sequence Spread-Spectrum Communications

As discussed in the previous chapter, multiuser receivers and joint detection can mitigate the effects of the MAI. However, these receivers require a considerable amount of knowledge about the MAI and can only operate at high computational costs.

In this thesis, it is shown that "code-on-pulse" modulation or "modulation on symbol" [14] can alleviate the impact of the MAI by exploiting the repetitive or *cyclic* nature of the signals.

Time-dependent filters perform better than time-independent filters if the signal of interest or the interference exhibits the property of *cyclostationarity*.

Cyclostationarity has been heavily discussed by Gardner [15, 16, 17]. The principle of cyclostationarity is discussed in Section 3.1 and 3.2. These sections are based on work done earlier by Holley [18]. In Section 3.3, it will be shown that the optimal time-dependent adaptive filter for despreading and demodulating a CDMA DS-SS signal is a single linear filter.

3.1   Principles of Cyclostationarity

A process $x(t)$ is said to be *cyclostationary* in the wide sense if its mean and autocorrelation are periodic with some periodicity, T_0, i.e.,

$$E[x(t)] = E[x(t + T_0)], \tag{15}$$

14

and

$$R_{xx}(t,\tau) = R_{xx}(t + T_0, \tau), \tag{16}$$

where $E(\cdot)$ is the expectation operator, and $R_{xx}(\tau)$ represents the autocorrelation function defined by

$$R_{xx}(t,\tau) = E\left\{x\left(t + \frac{\tau}{2}\right)x^*\left(t - \frac{\tau}{2}\right)\right\}. \tag{17}$$

The superscript, $*$, denotes complex conjugation.

If the autocorrelation function $R_{xx}(t)$ is periodic, then it can be described by its Fourier series representation,

$$R_{xx}(t,\tau) = \sum_{\alpha \in \bar{\alpha}} R_{xx}^\alpha(\tau)e^{j2\pi\alpha t}, \tag{18}$$

where the *cyclic autocorrelation* function with respect to a *cycle*-frequency, α, is defined as

$$R_{xx}^\alpha(\tau) = E\left\{x\left(t + \frac{\tau}{2}\right)x^*\left(t - \frac{\tau}{2}\right)e^{-j2\pi\alpha t}\right\}. \tag{19}$$

It is said that the process $x(t)$ contains *second-order periodicity* with frequency α, if and only if $R_{xx}^\alpha(\tau)$ exists and is not identically zero as a function of τ. The cyclic autocorrelation coefficients are determined by

$$R_{xx}^\alpha(\tau) = \lim_{T \to \infty} \frac{1}{T} \int_{-\frac{T}{2}}^{\frac{T}{2}} R_{xx}(t,\tau)e^{-j2\pi\alpha t}dt. \tag{20}$$

In Equation 18, the set $\bar{\alpha}$ denotes the set of all frequencies, α_n, for which $R_{xx}^\alpha \neq 0$. For purely cyclostationary signals, the cycle-frequencies are integrally related to a fundamental frequency,[1] α_0, for which

$$\alpha_0 = \frac{1}{T_0}. \tag{21}$$

Likewise, the *spectral correlation density function* can be defined which is analogous to the power spectrum for stationary signals. It can be viewed as the cross correlation between frequency components at $f - \alpha/2$ and $f + \alpha/2$. The spectral correlation density function, $S_{xx}^\alpha(f)$, is defined as

$$S_{xx}^\alpha(f) = \lim_{W \to \infty} \lim_{T \to \infty} \frac{1}{T} \int_{-\frac{T}{2}}^{\frac{T}{2}} \frac{1}{W} E\left\{X_W\left(t, f + \frac{\alpha}{2}\right)X_W^*\left(t, f - \frac{\alpha}{2}\right)\right\}dt, \tag{22}$$

where $X_W(t, f)$ is the Fourier transform of a finite window of data

$$X_W(t, f) = \int_{t-\frac{W}{2}}^{t+\frac{W}{2}} x(u)e^{-j2\pi fu}du. \tag{23}$$

---

[1]For some processes which show periodic behavior, the statistical periodicities are non-harmonically related. These processes are referred to as *almost cyclostationary*.

It can be shown that the spectral correlation density function and the cyclic autocorrelation function are a Fourier transform pair [17]. Hence, it is

$$S_{xx}^{\alpha}(f) = \int_{-\infty}^{\infty} R_{xx}^{\alpha}(\tau)e^{-j2\pi f\tau}d\tau. \tag{24}$$

It is recognized that the spectral correlation density function, $S_{xx}^{\alpha}(f)$, equals the conventional definition of the spectral density function $S_x(f)$ for $\alpha = 0$. Henceforth, $S_x(f)$ will be referred to as the *spectral density function* and $S_{xx}^{\alpha}(f)$ will be referred to as the *cyclic spectrum*.

The cyclic cross correlation of $y(t)$ and $x(t)$ is defined as

$$R_{yx}^{\alpha}(\tau) = \mathrm{E}\left\{y\left(t+\frac{\tau}{2}\right)x^*\left(t-\frac{\tau}{2}\right)e^{-j2\pi\alpha t}\right\}, \tag{25}$$

and the cross cyclic spectrum is

$$S_{yx}^{\alpha}(f) = \lim_{W\to\infty}\lim_{T\to\infty}\frac{1}{T}\int_{-\frac{T}{2}}^{\frac{T}{2}}\frac{1}{W}\mathrm{E}\left\{Y_W\left(t,f+\frac{\alpha}{2}\right)X_W^*\left(t,f-\frac{\alpha}{2}\right)\right\}dt. \tag{26}$$

The following sections discuss where and how DS-SS signals exhibit spectral correlation, and how the spectral correlation might be exploited to better reject interference and demodulate a desired signal.

3.2   Spectral Correlation in DS-SS Signals

The generation and description of a DS-SS signal is discussed in Section 1.2. The underlying statistical periodicities in a DS-SS signal have been investigated by Chen [19]. In his Ph.D. dissertation he showed the existence of three fundamental periodicities:

1. the chip period, T_c.

2. the data period, T_{data}.

3. the code repetition period, T_{code}.

For polar BPSK signaling, the data period is the bit period, T_b. The code repetition period is the period for which the spreading codes repeat.

Furthermore, Chen derived an expression for the cyclic autocorrelation functions $R_{xx}^{\alpha}(\tau)$ for a DS-SS signal

$$x(t) = c(t)d(t), \tag{27}$$

16

where $c(t)$ is the spreading waveform and $d(t)$ is the data waveform. The spreading waveform is described by

$$c(t) = \sum_{m=-\infty}^{\infty} c_m q\left(\frac{t}{T_c} - m\right),$$ (28)

where c_m are the chips taken from the alphabet $\{-1, 1\}$, and $q(t)$ is the rectangular function

$$q(t) = \begin{cases} 1, & -\frac{1}{2} \leq t \leq \frac{1}{2}, \\ 0, & \text{otherwise.} \end{cases}$$ (29)

In this derivation, it is assumed that the periodicities are harmonically related and that the spreading code repeats with an integer multiple of the bit period, i.e.,

$$\begin{aligned} T_{data} &= S T_c, \\ T_{code} &= N S T_c, \end{aligned}$$ (30)

where S and N are two integer numbers. The cyclic autocorrelation function for $x(t)$ is [19]

$$R_{xx}^\alpha(\tau) = \sum_{n,m=-\infty}^{\infty} C_n C_m^* R_{dd}^{\alpha - \frac{(n-m)}{NST_c}}(\tau) e^{-j\frac{\pi(n+m)\tau}{NST_c}},$$ (31)

where C_n represents a scaled version of the Fourier coefficients of the chip sequence waveform,

$$\begin{aligned} C_n &= \frac{1}{NST_c} \int_{-\frac{NST_c}{2}}^{\frac{NST_c}{2}} c(t) e^{-j\frac{2\pi nt}{NST_c}} dt \\ &= \frac{1}{NST_c} \int_{-\frac{NST_c}{2}}^{\frac{NST_c}{2}} \sum_{m=-\infty}^{\infty} c_m q\left(\frac{t}{T_c} - m\right) e^{-j\frac{2\pi nt}{NST_c}} dt \\ &= B_n \frac{\sin\left(\frac{\pi n}{NS}\right)}{\pi n}, \end{aligned}$$ (32)

where

$$B_n = \sum_{m=0}^{NS-1} c_m e^{-j\frac{2\pi nm}{NS}}.$$ (33)

Substituting Equation 31 into Equation 24, the expression for the cyclic spectrum can be obtained,

$$\begin{aligned} S_{xx}^\alpha(f) &= \sum_{n,m=-\infty}^{\infty} C_n C_m^* S_{dd}^{\alpha - \frac{(n-m)}{NST_c}}\left(f + \frac{n+m}{2NST_c}\right) \\ &= \sum_{n,l=-\infty}^{\infty} C_n C_m^* S_{dd}^{\alpha - \frac{l}{NST_c}}\left(f + \frac{n}{NST_c} - \frac{l}{2NST_c}\right). \end{aligned}$$ (34)

17

$S_{dd}^{\beta}(f)$ represents the cyclic spectral density of the baseband data signal, $d(t)$. The fundamental periodicity of $d(t)$ is the baud rate, T_{data} [16, 17]. The cycle frequencies β_m, $m = 0, \cdots, NS - 1$, of the data signal are the harmonics of the fundamental cycle frequency. Thus,

$$\beta_m = \frac{1}{T_{data}} = \frac{m}{ST_c}, \tag{35}$$

for all integer values m. It can be seen from Equations 35 and 34 that $S_{xx}^{\alpha}(f)$ is non-zero only for cycle frequencies α with

$$\alpha = \frac{l}{NST_c} + \frac{m}{ST_c}, \tag{36}$$

or

$$\alpha = \frac{l + mN}{NST_c} = \frac{p}{NST_c}, \tag{37}$$

where l, m, and p are integer numbers. For code-on-pulse modulation, i.e. $N = 1$, all cycle frequencies are harmonics of the code repetition cycle frequency.

3.3   Optimal Time-Dependent Filters in DS-SS

A linear filter transforms an observed signal, $x(t)$, into another signal, $\hat{y}(t)$,

$$\hat{y}(t) = \int_{-\infty}^{\infty} h(t, u) x(u)\, du. \tag{38}$$

Often, the observed signal, $x(t)$ is a corrupted form of an unobservable signal, $y(t)$. A filter can be used to remove the corruption in $x(t)$ such that the difference between the obtained output signal $\hat{y}(t)$ and the desired output $y(t)$ satisfies a certain error criterion. The most commonly used error criterion is *mean-squared error* (MSE), e, which can be expressed as

$$e = \mathrm{E}\left\{ |y(t) - \hat{y}(t)|^2 \right\}. \tag{39}$$

It can be shown that the optimal filter for purely stationary signals is time-independent,[2]

$$h(t, u) = h(t - u). \tag{40}$$

However, if the signals exhibit any kind of cyclostationarity the optimal filter is a periodically or almost periodically time-dependent filter [17, 20]. It is shown in Section 3.2 that a DS-SS signal is cyclostationary. Therefore, the optimal filter is a periodically time-dependent filter, $h(t, u)$. If the filter is periodically time-dependent with fundamental periodicity, T_{data}, it can be expressed by its *Fourier series representation* (FSR),

$$h(t, u) = \sum_{\beta \in \bar{\beta}} g_\beta(t - u) e^{j2\pi\beta ut}, \tag{41}$$

---

[2]This filter is known as the Wiener filter.

18
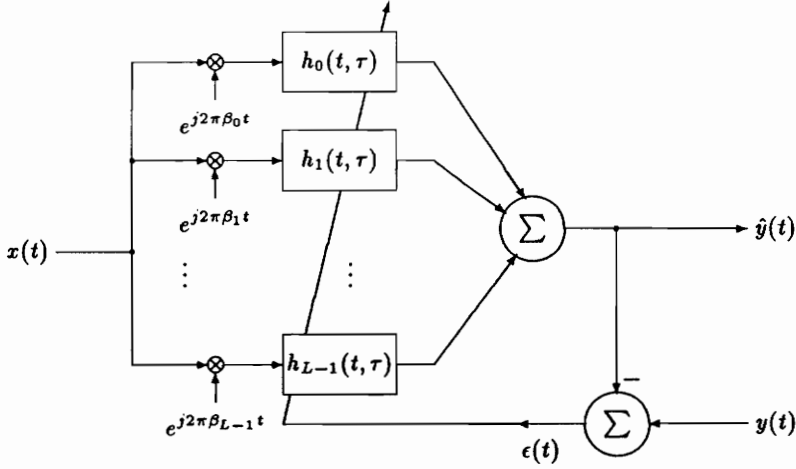
Figure 11: FSR time-dependent adaptive filter.

where $\bar{\beta}$ is the set of cycle frequencies for which $g_\beta(\tau) \neq 0$ for all τ. Substituting Equation 41 into 38 yields

$$\hat{y}(t) = \sum_{\beta \in \bar{\beta}} g_\beta(t) * \left[x(t) e^{j2\pi\beta t} \right].$$ (42)

From Equation 42, it can be seen that $\hat{y}(t)$ is the sum of linear time-independent filtered versions of complex frequency shifted time-series,

$$x_\beta(t) = x(t) e^{j2\pi\beta t}.$$ (43)

Equation 42 directly shows how to implement the time-dependent filter. Since the filter is based on the FSR, it is referred to as the *FSR time-dependent filter* (FSR TDF). A version of the *FSR time-dependent adaptive filter* (FSR TDAF) is illustrated in Figure 11 [21, 22, 20]. First, the input signal is multiplied by the different carriers, $e^{j2\pi\beta_i t}$, for all cycle frequencies, β_i, for $0 \le i \le L - 1$. Each frequency-shifted replica of the signal is passed through a different filter with frequency response $h_i(\tau, t)$ and summed to form the output. An adaptation algorithm compares the output, $\hat{y}(t)$ with a desired signal, $y(t)$, and adjusts the filters to minimize the MSE. The design equation which determines the filter responses, $g_\beta(u)$, and minimizes the MSE is [17]

$$R_{yx}^{\alpha}(u) e^{j\pi\beta u} = \sum_{\beta \in \bar{\beta}} g_\beta(u) * \left[R_x^{(\alpha-\beta)}(u) e^{j\pi(\alpha+\beta)u} \right],$$ (44)

for all u and α of interest. If an optimum periodically time-variant filter is desired, then the sets $\bar{\alpha}$ and $\bar{\beta}$ must contain all integer multiples of the fundamental cycle frequency. The

19
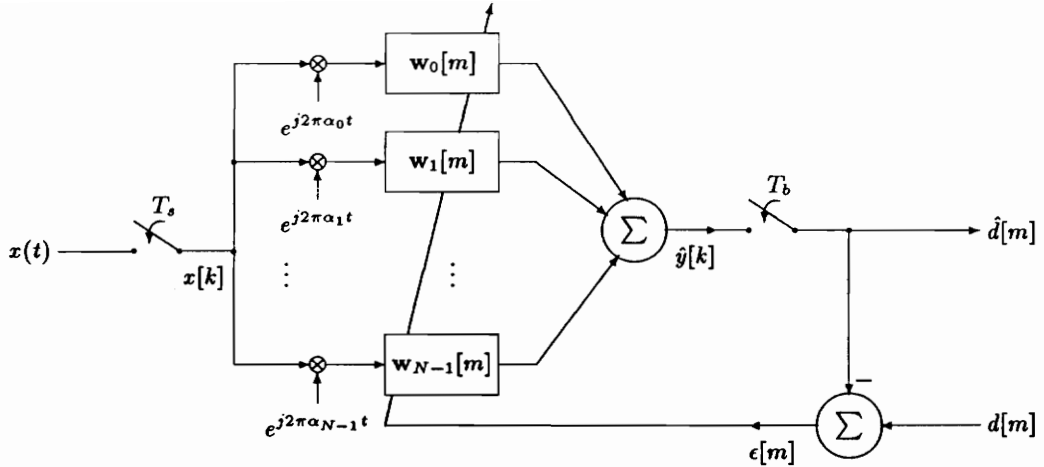
Figure 12: The discrete-time FSR SE.

minimum attainable MSE for Equation 44 is

$$e_{\min} = R_y^0(0) - \sum_{\beta \in \bar{\beta}} \int_{-\infty}^{\infty} g_\beta(u) \left[R_{yx}^\beta(u) e^{j\pi\beta u} \right]^* du. \qquad (45)$$

The FSR TDAF can also be used to estimate the waveform of a corrupted BPSK DS-SS signal. Versions of the FSR TDAF for interference cancellation of DS-SS have been investigated by J. H. Reed [23] and R. D. Holley [18]. Based on a discrete Fourier transform implementation, their algorithms estimate the uncorrupted signal $\hat{y}(t)$.

If $\hat{y}(t)$ can be described by

$$\hat{y}(t) = y(t) + n(t), \qquad (46)$$

$n(t)$ is white noise, then the optimal filter for demodulating $\hat{y}(t)$ is the matched filter as described in Section 2.1.

However, since the matched filter is another linear filter, it might be included into the filter impulse responses $h_i(t, \tau)$, $i = 0, 1, \cdots, L - 1$. The output at every instant nT_b, where T_b is the bit period and n is an integer number, can be used to estimate the transmitted data bits, $d[n]$. The so obtained filter is referred to as the *FSR sequence estimator* (FSR SE). The discrete-time version of the FSR SE is pictured in Figure 12. It is assumed that the filters for each frequency shift are *finite impulse response* (FIR) filters of length l. They are represented by their coefficient vector $\mathbf{w}_i[m]$, with the coefficients $w_{i,n}$, for $0 \leq n \leq l-1$. Figure 13 shows the FIR filter of the ith user. The weights are updated at $t = mT_b$.

The discrete-time series, $x[k]$, resulting from sampling the continuous signal, $x(t)$, with

20
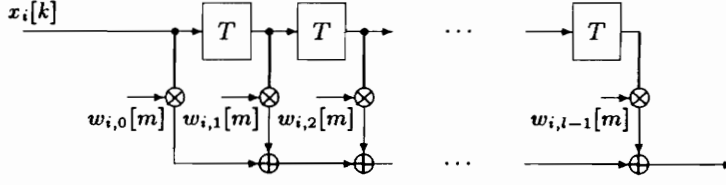
Figure 13: FIR filter of the ith user.

sampling period T_s is defined as

$$x[k] = x(kT_s). \tag{47}$$

The output of the FSR SE after subsampling behind the summer is the estimated data symbol $\hat{d}[m]$. The error $\epsilon[m]$ is the difference between the estimated data symbol $\hat{d}[m]$ and the desired data symbol, $d[m]$.

In the following, it is shown that the FIR filters in Figure 12 can be combined to a single FIR filter. For this, it is assumed that the bit period, T_b, is an integer multiple of the sampling period T_s,

$$T_b = NT_s. \tag{48}$$

The set of cycle frequencies, $\bar{\alpha}$ which can be exploited by the FSR SE for the discrete-time case is

$$\bar{\alpha} = \{0, \alpha_0, 2\alpha_0, \cdots, (N-1)\alpha_0\}. \tag{49}$$

It was mentioned earlier that for a DS-SS BPSK signaling scheme which satisfies Equation 30, the fundamental periodicity, α_0, is the bit rate R_b, i.e.,

$$\alpha_0 = \frac{1}{T_b}. \tag{50}$$

The estimated time series $\hat{y}[k]$ can be expressed by

$$
\begin{aligned}
\hat{y}[k] &= \sum_{n=0}^{N-1} w_{n,k}[m] * \left(x[k] e^{j2\pi n\alpha_0 kT_s} \right) \\
&= \sum_{n=0}^{N-1} w_{n,k}[m] * \left(x[k] e^{j\frac{2\pi}{N}nk} \right).
\end{aligned}
\tag{51}
$$

For every sample $k = mN$, the convolution inside the summation is

$$
\begin{aligned}
w_{n,k}[m] * \left(x[k] e^{j\frac{2\pi}{N}nk} \right) &= \sum_{p=0}^{l-1} w_{n,p}[m] x[mN - p] e^{j\frac{2\pi}{N}n(mN-p)} \\
&= \sum_{p=0}^{l-1} w_{n,p}[m] x[mN - p] e^{-j\frac{2\pi}{N}np}.
\end{aligned}
\tag{52}
$$

21

Thus, Equation 51 becomes

$$\hat{y}[mN] = \sum_{n=0}^{N-1} \sum_{p=0}^{l-1} w_{n,p}[m] x[mN - p] e^{-j\frac{2\pi}{N}np}. \tag{53}$$

Exchanging the order of summation yields

$$\hat{y}[mN] = \sum_{p=0}^{l-1} x[mN - p] \sum_{n=0}^{N-1} w_{n,p}[m] e^{-j\frac{2\pi}{N}np}. \tag{54}$$

The second summation can be recognized as the Fourier transform,

$$\tilde{w}_p[m] = \sum_{n=0}^{N-1} w_{n,p}[m] e^{-j\frac{2\pi}{N}np}. \tag{55}$$

Then, Equation 54 can be rewritten as

$$\hat{y}[mN] = \sum_{p=0}^{l-1} \tilde{w}_p[m] x[mN - p]. \tag{56}$$

Since $\hat{y}[mN] = \hat{d}[m]$ are the estimated data bits $\hat{d}[m]$, it can be concluded that a single linear filter with tap-spacing T_s harmonically related to the bit rate T_b is the optimal time-dependent filter for demodulating a BPSK DS-SS signal and it is capable of exploiting its cyclostationarity.

Chapter 4

Optimum Linear Single User Detection in DS-SS

It is shown in Section 2.1 that a linear transversal filter can be used to demodulate and despread a DS-SS. Section 3.3 shows that a linear transversal filter is the optimum time-dependent filter for a DS-SS signal employing code on pulse modulation. This chapter discusses possible implementations of the optimum linear single user receiver.

4.1 Preliminaries

Consider the block diagram of the FIR filter depicted in Figure 14. As described in Section 3.3, for the demodulation process, it is sufficient to calculate the output for each complete bit shifted into the tapped delay line. It is assumed that the length of the tapped delay line, M, is sufficiently large to hold an entire bit,
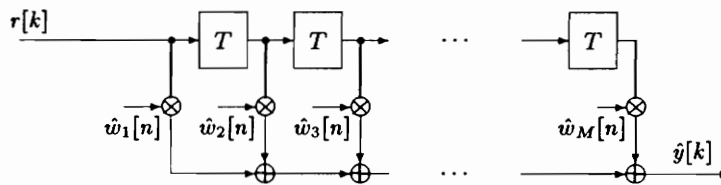
$$MT_s \geq T_b. \tag{57}$$

Figure 14: Block diagram of the FIR filter.

Let $r[k]$ denote the discrete-time series resulting from sampling a continuous signal $r(t)$ with sampling period T_s,

$$r[k] = r(kT_s). \tag{58}$$

It is convenient to define the vector for the samples which correspond to the nth bit as

$$\hat{\mathbf{r}}[n] = \begin{bmatrix} r[nN] & r[nN-1] & \cdots & r[nN-M+1] \end{bmatrix}^T, \tag{59}$$

where N is defined as

$$N = \frac{T_b}{T_s}. \tag{60}$$

The weight vector, $\mathbf{w}[n]$, contains the weights of the filter in Figure 14 and is defined as

$$\hat{\mathbf{w}}[n] = \begin{bmatrix} \hat{w}_1[n] & \hat{w}_2[n] & \cdots & \hat{w}_M[n] \end{bmatrix}^T. \tag{61}$$

This vector is used to form an estimate of the desired bit, $d[n]$, by calculating the inner product $\hat{\mathbf{w}}^H[n]\hat{\mathbf{r}}[n]$,

$$d[n] = \hat{\mathbf{w}}^H[n]\hat{\mathbf{r}}[n] + \hat{\epsilon}[n], \tag{62}$$

where $\hat{\epsilon}[n]$ is the complex estimation error. The superscript, H, denotes transpose conjugate.

For BPSK DS-SS signaling, the transmitted symbols are $+1$ and -1. Using the imaginary axis as the decision boundary, the estimated symbol, $\tilde{d}[n]$, is

$$\tilde{d}[n] = \begin{cases} -1, & \mathrm{Re}\big\{\hat{\mathbf{w}}^H[n]\hat{\mathbf{r}}[n]\big\} < 0, \\ +1, & \mathrm{Re}\big\{\hat{\mathbf{w}}^H[n]\hat{\mathbf{r}}[n]\big\} > 0. \end{cases} \tag{63}$$

It is desirable to adjust the weight vector such that the likelihood of making a false decision is minimized.

4.2 Decoupling the Real and Imaginary Filter Coefficients

Here, the justification for decoupling the real and imaginary filter coefficients is given.

The conventional estimation error for a desired data symbol, $d[n]$, is given in Equation 62. The estimated symbol is

$$\hat{d}[n] = \hat{\mathbf{w}}^H[n]\hat{\mathbf{r}}[n]. \tag{64}$$

Figure 15 shows the constellation diagram of a BPSK signal and the error between an estimated signal point $\hat{d}[n]$ and the desired signal point $d[n]$.

The most commonly used error-criterion for adjusting the weight vector is the mean-squared error,

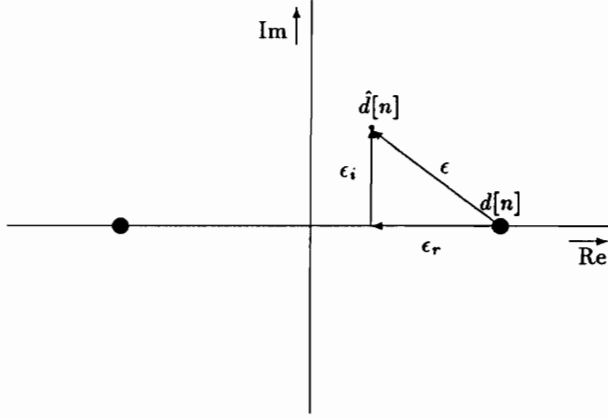$$\hat{e} = \mathrm{E}\big\{|\hat{\epsilon}[n]|^2\big\}, \tag{65}$$

Figure 15: Signal constellation diagram for a BPSK signal.

where $E(\cdot)$ is the expectation operator. According to Equation 63, however, the decision is based only on the real part of the inner product $\hat{\mathbf{w}}^H[n]\hat{\mathbf{r}}[n]$. Finding the optimum weight vector for minimizing Equation 65 would result in minimizing the real error, ϵ_r, and the imaginary error, ϵ_i. However, since the decision on $\hat{d}[n]$ depends only on the real part of the filtered signal and minimizing the imaginary part reduces the ability to minimize the real part, the only error to be considered should be the real error, ϵ_r. This error is more reflective of the BER than the complex error. Minimizing the MSE for ϵ_r can be easily accomplished by using the following matrix notation to calculate the inner product $\hat{\mathbf{w}}^H\hat{\mathbf{r}}[n] = a[n] + jb[n]$.

$$
\begin{bmatrix}
\mathrm{Re}\{\hat{\mathbf{w}}^H\} & -\mathrm{Im}\{\hat{\mathbf{w}}^H\} \\
\mathrm{Im}\{\hat{\mathbf{w}}^H\} & \mathrm{Re}\{\hat{\mathbf{w}}^H\}
\end{bmatrix}
\begin{bmatrix}
\mathrm{Re}\{\hat{\mathbf{r}}[n]\} \\
\mathrm{Im}\{\hat{\mathbf{r}}[n]\}
\end{bmatrix}
=
\begin{bmatrix}
a[n] \\
b[n]
\end{bmatrix},
\tag{66}
$$

where $a[n]$ and $b[n]$ are two real numbers, and $a[n]$ represents the real part and $b[n]$ represents the imaginary part of the product $\hat{\mathbf{w}}^H\hat{\mathbf{r}}[n]$. Since the imaginary part, $b[n]$, is neither used for the error-criterion nor for deciding on $\hat{d}[n]$, it does not need to be calculated.

It is convenient to define the $2M$-by-1 real weight vector $\mathbf{w}[n]$,

$$
\mathbf{w}[n] =
\begin{bmatrix}
\mathrm{Re}\{\hat{\mathbf{w}}[n]\} \\
\mathrm{Im}\{\hat{\mathbf{w}}[n]\}
\end{bmatrix},
\tag{67}
$$

and the $2M$-by-1 real vector,

$$
\mathbf{r}[n] =
\begin{bmatrix}
\mathrm{Re}\{\hat{\mathbf{r}}[n]\} \\
\mathrm{Im}\{\hat{\mathbf{r}}[n]\}
\end{bmatrix}.
\tag{68}
$$

Thus, the decision variable, $a[n]$, can be expressed by

$$
a[n] = \mathbf{w}^T[n]\mathbf{r}[n],
\tag{69}
$$

25
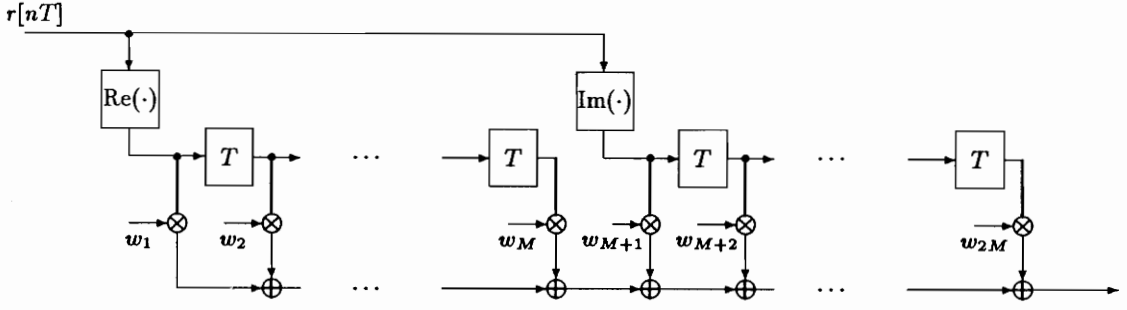
Figure 16: FIR filter with real weights.

where the superscript, T, denotes transposition. The desired data symbols are

$$d[n] = \mathbf{w}^T[n]\mathbf{r}[n] + \epsilon[n], \tag{70}$$

where $\epsilon[n]$ is the real error. Minimizing the mean-squared error for Equation 70 is the desired criterion for finding the optimum weight vector. The FIR filter using the real valued weight vector is illustrated in Figure 16.

It should be mentioned that this consideration can be extended to QPSK signaling. For QPSK signaling, substantial improvement over solving the complex normal equations can be gained, if the normal equations are solved for $a[n]$ and $b[n]$ individually. However, in so doing, more storage size is required, since two different weighting vectors need to be obtained.

4.3   Optimum CDMA DS-SS Filtering

It is stated in the previous section that the weight vector of the FIR filter in Figure 16 should minimize the MSE for Equation 70.

The error $\epsilon[n]$ is defined as

$$\epsilon[n] = d[n] - \mathbf{w}^T\mathbf{r}[n]. \tag{71}$$

The weights are determined by minimizing the MSE $J(\mathbf{w})$ which is

$$J(\mathbf{w}) = \mathrm{E}\left\{\left(\epsilon[n]\right)^2\right\}, \tag{72}$$

where $\mathrm{E}(\cdot)$ defines the expectation operator. Substituting Equation 71 into yields

$$
\begin{aligned}
J(\mathbf{w}) &= \mathrm{E}\left\{\left(d[n] - \mathbf{w}^T\mathbf{r}[n]\right)^2\right\} \\
&= \mathrm{E}\left\{\left(d[n]\right)^2 - 2d[n]\mathbf{w}^T\mathbf{r}[n] + \mathbf{w}^T\mathbf{r}[n]\mathbf{r}^T[n]\mathbf{w}\right\}. \tag{73}
\end{aligned}
$$

26

Since the expectation operator is a linear operator, and since $\mathbf{w}$ is constant, $J(\mathbf{w})$ can be expressed by

$$J(\mathbf{w}) = E\left\{(d[n])^2\right\} - 2\mathbf{w}^T E\big(d[n]\mathbf{r}[n]\big) + \mathbf{w}^T E\big(\mathbf{r}[n]\mathbf{r}^T[n]\big)\mathbf{w}. \tag{74}$$

The first term of Equation 74 can be recognized as the variance σ_d^2 of the data $d[n]$, i.e.,

$$\sigma_d^2 = E\left\{(d[n])^2\right\}. \tag{75}$$

The second expectation operator equals the $2M$-by-1 cross-correlation vector $\mathbf{p}$ between the input vector $\mathbf{r}[n]$ and the desired output $d[n]$,

$$\mathbf{p} = E\big(d[n]\mathbf{r}[n]\big), \tag{76}$$

and $E\big(\mathbf{r}[n]\mathbf{r}^T[n]\big)$ equals the $2M$-by-$2M$ correlation matrix $\mathbf{R}$, i.e.,

$$\mathbf{R} = E\big(\mathbf{r}[n]\mathbf{r}^T[n]\big). \tag{77}$$

Thus, Equation 74 can be rewritten as

$$J(\mathbf{w}) = \sigma_d^2 - 2\mathbf{w}^T\mathbf{p} + \mathbf{w}^T\mathbf{R}^T\mathbf{w}. \tag{78}$$

The requirements for the vector $\mathbf{w}_o$ which minimizes $J(\mathbf{w})$ is

$$\frac{dJ(\mathbf{w}_o)}{d\mathbf{w}_o} = \mathbf{0}. \tag{79}$$

By defining the derivative of a scalar valued function, $f(\mathbf{w})$, with respect to a $2M$-by-1 vector, $\mathbf{w}$, as,

$$\frac{df(\mathbf{w})}{d\mathbf{w}} = \begin{bmatrix} \frac{\partial f(\mathbf{w})}{\partial w_1} \\ \frac{\partial f(\mathbf{w})}{\partial w_2} \\ \vdots \\ \frac{\partial f(\mathbf{w})}{\partial w_{2M}} \end{bmatrix}, \tag{80}$$

the derivatives of the terms in Equation 78 are

$$\frac{d}{d\mathbf{w}}(\mathbf{w}^T\mathbf{p}) = \mathbf{p} \tag{81}$$

$$\frac{d}{d\mathbf{w}}(\mathbf{w}^T\mathbf{R}\mathbf{w}) = 2\mathbf{R}\mathbf{w}. \tag{82}$$

The derivative of the constant term σ_d^2 equals zero. Therefore, the derivative of Equation 78,

$$\frac{dJ(\mathbf{w})}{d\mathbf{w}} = -2\mathbf{p} + 2\mathbf{R}\mathbf{w}, \tag{83}$$

27

and substituting into Equation 79 yields the desired result

$$\mathbf{R}\mathbf{w}_o = \mathbf{p}. \tag{84}$$

This result is most commonly referred to as the *normal equation* [24]. By premultiplying Equation 84 with the inverse correlation matrix $\mathbf{R}^{-1}$, the desired vector $\mathbf{w}_o$ is obtained:

$$\mathbf{w}_o = \mathbf{R}^{-1}\mathbf{p}. \tag{85}$$

Minimum Mean-Squared Error

Assuming the optimum weight vector and the data have zero mean, the variance of the estimated data, $\hat{d}[n]$, is

$$
\begin{aligned}
\sigma_{\hat{d}}^2 &= \mathrm{E}\left[\mathbf{w}_o^T \mathbf{r}[n]\mathbf{r}^T[n]\mathbf{w}_o\right] \\
&= \mathbf{w}_o^T \mathbf{R}\mathbf{w}_o.
\end{aligned}
\tag{86}
$$

Substituting Equation 84 and 85 into Equation 86 yields

$$
\begin{aligned}
\sigma_{\hat{d}}^2 &= \mathbf{w}_o^T \mathbf{p} \\
&= \mathbf{p}^T \mathbf{R}^{-1}\mathbf{p}.
\end{aligned}
\tag{87}
$$

Using the corollary of the principle of orthogonality [24], the minimum attainable MSE produced by the filter in Figure 16 is

$$e_{\min} = \sigma_d^2 - \mathbf{p}^T \mathbf{R}^{-1}\mathbf{p}, \tag{88}$$

where σ_d^2 is the standard deviation of the data given by Equation 75.

4.4   Optimum Single User Receiver Implementations

The implementation of the optimum single-user DS-SS detector is depicted in Figure 17. The detector employs the decoupled real and imaginary filter weights as discussed in Section 4.3 and shown in Figure 16. By multiplying the outputs of the tapped delay line with the corresponding weight factors w_i, for $1 \le i \le 2M$, and summing the products, the inner product $\mathbf{w}^T[n]\mathbf{r}[n]$ is formed giving an estimate of the transmitted data, $d[n]$. The estimated data is hard-limited to provide a decision for the symbol. The hard-limiting function, $f_{\mathrm{HL}}(y)$, can be described by

$$f_{\mathrm{HL}}(y) = \begin{cases} 1, & y \ge 0, \\ -1, & y < 0. \end{cases} \tag{89}$$
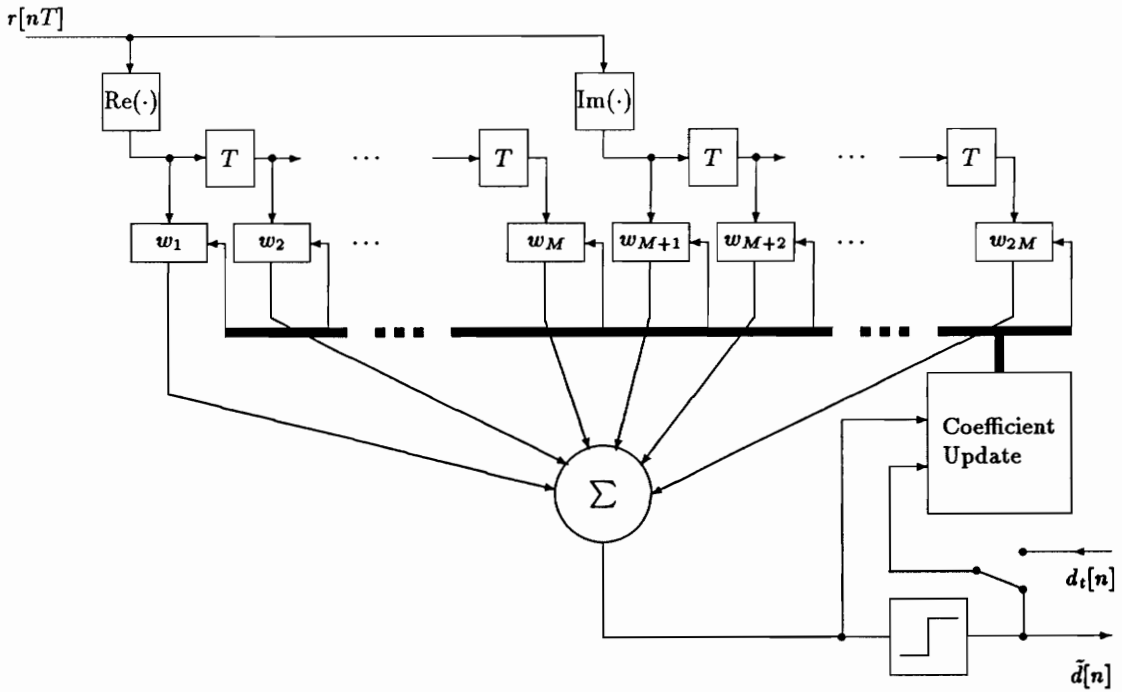
Figure 17: Optimum single-user DS-SS detector.

A *coefficient update* algorithm compares the output of the summer with the desired response $d[n]$ to form an error signal. The coefficient update algorithm updates the weight vector $\mathbf{w}[n]$ to minimize the error-criterion. Referring to Section 4.3, the error-criterion used here is the mean-squared error,

$$e = \mathrm{E}\Big\{ \big(\mathbf{w}^T[n]\mathbf{r}[n] - d[n]\big)^2 \Big\}. \tag{90}$$

In a real communication system, the data bits, $d[n]$, are usually unknown at the receiver. Two approaches are generally used to estimate the error, $\epsilon[n]$:

1. In *decision-directed* mode, the estimated and hard-limited data bits $\tilde{d}[n]$ are taken as the desired response. This assumes a high likelihood of correct decisions by the hard-limiter.

2. If the decisions are not highly likely to be correct, e.g., during the initialization period, where the weight vector $\mathbf{w}[n]$ has not yet converged to its optimal value, a *training sequence*, $d_t[n]$, must be used to train the filter until the estimates are of high quality and the decision-directed mode becomes feasible. The training sequence consists of a set of consecutive bits, known at the transmitter and receiver.

29

Note the similarities between the receiver unit shown in Figure 16 and an ordinary fractionally spaced linear decision feedback equalizer.

However, the differences lie in the application and the system setup. The equalizer attempts to compensate for the effects of the channel, whereas this receiver tries to equalize, reject interference, and demodulate in "one shot" exploiting the periodicities of the SOI and the *signal not of interest* (SNOI).

4.4.1 Recursive Least-Squares Implementation

The algorithm discussed in this paragraph recursively solves the normal equations for each new observed data sample $d[n]$, hence the name *recursive least-squares* (RLS) algorithm. The following gives a brief description of the *weighted* RLS algorithm. For a detailed discussion, the reader is referred to reference [25].

Equation 85 gives an expression for calculating the weighting vector, $\mathbf{w}$. In a real system, however, the correlation matrix, $\mathbf{R}$, and the cross-correlation vector, $\mathbf{p}$, are calculated from a finite number of observations, n. Also, if the statistics of the observed signal are slowly time-varying, it is helpful to introduce the weighted deterministic correlation matrix, $\mathbf{\Phi}[n]$, with

$$\mathbf{\Phi}[n] = \sum_{i=1}^{n} \lambda^{n-i} \mathbf{u}[n]\mathbf{u}^{T}[n] \tag{91}$$

where $0 < \lambda \leq 1$ is a constant also referred to as the *forgetting factor*. Likewise, the deterministic cross-correlation vector, $\mathbf{\Theta}[n]$, is defined as

$$\mathbf{\Theta}[n] = \sum_{i=1}^{n} \lambda^{n-i} \mathbf{u}[i]d[i]. \tag{92}$$

The forgetting factor insures an exponential decaying weighting of the observations. Equation 91 and 92 have a recursive form,

$$\mathbf{\Phi}[n] = \lambda\mathbf{\Phi}[n-1] + \mathbf{u}[n]\mathbf{u}^{T}[n], \tag{93}$$

$$\mathbf{\Theta}[n] = \lambda\mathbf{\Theta}[n-1] + \mathbf{u}[n]d[n]. \tag{94}$$

By making use of the matrix inversion lemma, an inversion of the deterministic correlation matrix at each iteration can be avoided.

The matrix inversion lemma states that

$$\mathbf{A}^{-1} = \mathbf{B} - \mathbf{B}\mathbf{C}(\mathbf{D} + \mathbf{C}^{H}\mathbf{B}\mathbf{C})^{-1}\mathbf{C}^{H}\mathbf{B}, \tag{95}$$

for

$$\mathbf{A} = \mathbf{B}^{-1} + \mathbf{C}\mathbf{D}^{-1}\mathbf{C}^{H}, \tag{96}$$

Table 1: The RLS algorithm

Initialization of the algorithm

$$\lambda = \text{constant}, \quad 0 < \lambda \leq 1$$

$$\mathbf{w}[0] = \mathbf{0}$$

$$\mathbf{\Phi}^{-1}[n] = \eta \cdot \mathbf{I}, \quad \eta \text{ is a very large constant}$$

For each instant n of time nT_b compute

$$\hat{d}[n] = \mathbf{w}^T[n-1]\mathbf{r}[n]$$

$$\alpha[n] = d[n] - \hat{d}[n]$$

$$\mathbf{z}^T[n] = \mathbf{r}^T[n]\mathbf{\Phi}^{-1}[n-1]$$

$$Q = \mathbf{z}^T[n]\mathbf{r}[n]$$

$$V = \frac{1}{\lambda + Q}$$

$$\tilde{\mathbf{z}}[n] = V \cdot \mathbf{\Phi}^{-1}[n-1]\mathbf{r}[n]$$

$$\mathbf{\Phi}^{-1}[n] = \frac{1}{\lambda}\left(\mathbf{\Phi}^{-1}[n-1] - \tilde{\mathbf{z}}[n]\mathbf{z}^T[n]\right)$$

$$\mathbf{w}[n] = \mathbf{w}[n-1] + \alpha[n]\tilde{\mathbf{z}}[n]$$

---

where $\mathbf{A}$ and $\mathbf{B}$ are two positive definite, M-by-M matrices, $\mathbf{C}$ is an M-by-N matrix, and $\mathbf{D}$ is another positive definite, N-by-N matrix. By setting

$$
\begin{aligned}
\mathbf{A} &= \mathbf{\Phi}[n], \\
\mathbf{B}^{-1} &= \lambda\mathbf{\Phi}[n-1], \\
\mathbf{C} &= \mathbf{r}[n], \\
\mathbf{D} &= 1,
\end{aligned}
$$

the equations for the RLS algorithm are obtained.

Table 1 summarizes the RLS algorithm. It begins with selecting the forgetting factor λ. This factor determines the influence of previous observations on the correlation matrix, $\mathbf{\Phi}[n]$, as described by Equation 91. For $\lambda = 1$ each observation is weighted evenly. By setting $\lambda = 1$, the algorithm gives an exact solution to the normal equations. However, in a time-varying channel it is desirable to let the weighting vector, $\mathbf{w}[n]$, track the varying channel. Hence, it is desirable to weight last observations more heavily. A good trade-off between error minimization and tracking performance for most scenarios is found for choosing λ such that

$$\lambda^{4M} \leq 0.01, \tag{97}$$

where $2M$ is the length of the vectors $\mathbf{w}[n]$ and $\mathbf{r}[n]$. With this setup, the impact of the vector $\mathbf{r}[n]$ on the correlation matrix after $4M$ iterations is less than one percent.

If no prior knowledge about the weighting vector $\mathbf{w}[n]$ is given, it is initially set to zero. Also, the correlation matrix is set to the identity matrix multiplied by a small factor. Thus, the initialization of the inverse correlation matrix is accomplished by setting $\mathbf{\Phi}[0]$ equal to the $2M$-by-$2M$ identity matrix, $\mathbf{I}$, times a large constant, η.

After initialization, based on the previous weighting vector $\mathbf{w}[n-1]$, the estimated data symbol $\hat{d}[n]$ is calculated at each iteration,

$$\hat{d}[n] = \mathbf{w}^T[n-1]\mathbf{r}[n]. \tag{98}$$

The difference between $\hat{d}[n]$ and the desired data symbol, $d[n]$, is the *a priori* error,

$$\alpha[n] = d[n] - \hat{d}[n]. \tag{99}$$

The so called *gain vector*, $\mathbf{z}^T[n]$, is used to update the inverse correlation matrix. It is calculated by

$$\mathbf{z}^T[n] = \mathbf{r}^T[n]\mathbf{\Phi}^{-1}[n-1]. \tag{100}$$

The normalized gain vector is obtained by

$$\tilde{\mathbf{z}}[n] = V \cdot \mathbf{\Phi}^{-1}[n-1]\mathbf{r}[n], \tag{101}$$

where the normalization parameters Q and V are given by

$$Q = \mathbf{z}^T[n]\mathbf{r}[n], \tag{102}$$

and

$$V = \frac{1}{\lambda + Q}. \tag{103}$$

Updating the inverse correlation matrix from the previous inverse correlation matrix takes place by subtracting a matrix formed by the product of $\mathbf{z}[n]$ and the *normalized gain vector*, $\tilde{\mathbf{z}}[n]$,

$$\mathbf{\Phi}^{-1}[n] = \frac{1}{\lambda}\left(\mathbf{\Phi}^{-1}[n-1] - \tilde{\mathbf{z}}[n]\mathbf{z}^T[n]\right). \tag{104}$$

Finally, the new weight vector is obtained by

$$\mathbf{w}[n] = \mathbf{w}[n-1] + \alpha[n]\tilde{\mathbf{z}}[n]. \tag{105}$$

This algorithm has been proven by Haykin [25] to be stable. The algorithm typically converges in $4M$ iterations to the optimum weight vector. This is considerably faster than the convergence rate of other algorithms.

One of the greatest disadvantages of the RLS algorithm is its relatively high computational complexity. Also, enough memory for the storage of the $2M$-by-$2M$ inverse correlation matrix $\Phi^{-1}[n]$ is needed. However, the RLS algorithm typically converges one order of magnitude faster than the *least mean-squares* (LMS). In non-stationary environments like in the mobile channel, fast convergence becomes crucial and added complexity of the use of the RLS algorithm over the LMS algorithm can be justified [26].

4.4.2 Operation of the RLS Algorithm Using Decision-Feedback

The RLS algorithm requires a desired data symbol, $d[n]$, to build the error term. This desired data symbol is supplied by either the training sequence or the hard-limiter. The RLS algorithm weights the updates regardless of the likelihood that a false decision on the symbol $\tilde{d}[n]$ is made. Using too many false decisions results in "catastrophic failure," i.e., the algorithm looses its tracking ability and fails to converge. A technique to overcome these problems is a modification in the algorithm investigated by R. D. Holley and J. H. Reed [18]. The modification takes place by introducing an update weighting function, $\Psi[n]$, in Equation 105

$$\mathbf{w}[n] = \mathbf{w}[n-1] + \Psi[n]\alpha[n]\tilde{\mathbf{z}}[n], \tag{106}$$

where $\Psi[n]$ is typically in the range $0 \leq \Psi[n] \leq 1$. Applying such a function, the weight vector $\mathbf{w}[n]$ in Equation 105 is now updated depending on the likelihood of a right decision. As a criterion, the difference between $\hat{d}[n]$ and the data $\tilde{d}[n]$ after symbol decision is used. Figure 18 depicts two candidate weighting functions, $f_w(x)$ and $f_e(x)$, for the BPSK signaling case. The weighting function $f_w(x)$ notches out the interval from $-0.5 \leq x \leq 0.5$; the function $f_e(x)$ uses two Gaussian shaped exponentials to define the weighting for updating the vector $\mathbf{w}[n]$. Other functions are possible. In general, it can be said that the probability for a catastrophic failure shrinks, with a more restrictive window. However, the more restrictive the window is, the slower the algorithm converges. The optimum weighting function depends on the input signal.

4.4.3 Sampling Rate

In a real bandpass system, the bandwidth of a BPSK DS-SS is limited. In most real world systems, only the mainlobe is transmitted. The sidelobes are usually filtered at the transmitter to increase spectral efficiency and at the receiver to decrease the noise power. The bandwidth $2B$ for the mainlobe of a BPSK DS-SS is
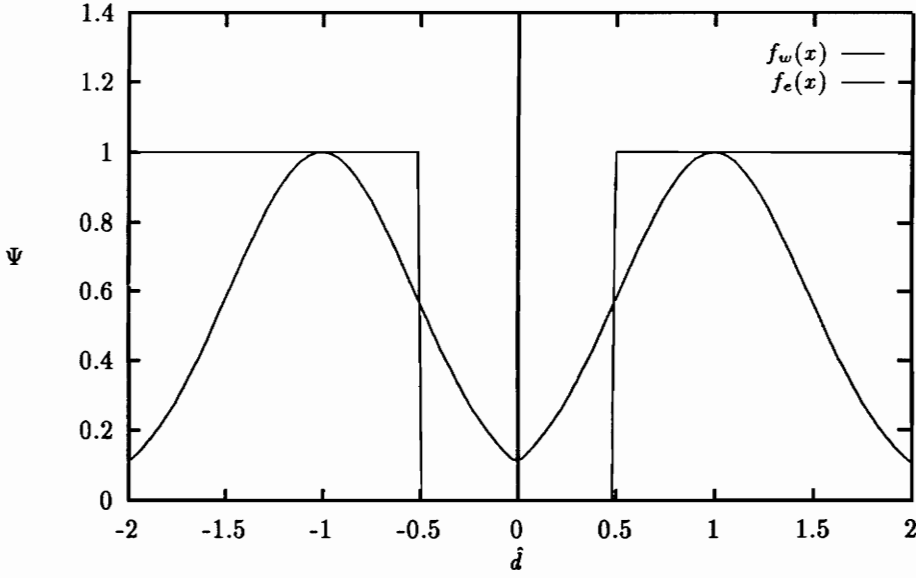
$$2B = 2R_b N, \tag{107}$$

Figure 18: Two candidate functions for $\Psi(x)$.

where $R_b = 1/T_b$ denotes the bit rate and N is the processing gain. Therefore, the sampling rate, f_s, should be set to $2B$ for complex samples. Thus, the tap spacing, $T_s = 1/f_s$, becomes

$$
\begin{aligned}
T_s &= \frac{1}{2R_bN} \\
&= \frac{T_c}{2},
\end{aligned}
\tag{108}
$$

where $1/T_c = NR_b$ is the chip rate. Also, higher sampling frequencies can be used. However, to exploit spectral correlation the sampling frequency must be an integer multiple of the bit rate, i.e.,

$$
f_s = lR_b,
\tag{109}
$$

where l is an integer.

4.4.4 Final Optimum Single User Receiver Implementations

Implementations of the optimum single user detector may vary. A possible solution which could be used for implementation at the base or at the mobile station is shown in Figure 19. A high-frequency pre-amplifier amplifies the received signal from the antenna. The pre-amplifier block includes bandpass filters to reject noise outside the information spectrum. A down converter applied to the output of the pre-amplifier followed by an analog-to-digital
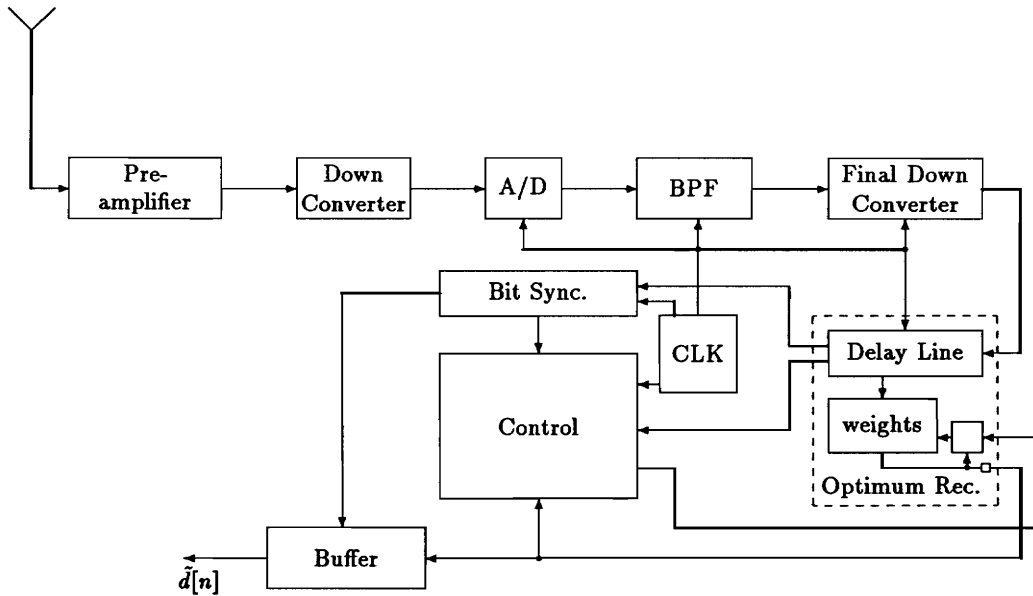
34

Figure 19: Final implementations of the optimum single user detector.

(A/D) converter down-shifts the signal, digitizes and samples it. After passing the discrete signal through another *bandpass filter* (BPF), the signal is shifted by a final down-converter to baseband. The signal is stored in a tapped delay line. The real and imaginary parts are then linearly combined as described in the introduction of Section 4.4. The dashed box (see also Figure 17) includes an implementation of the RLS algorithm and the hard-limiting function.

A control unit connected to the output of the receiver performs all the control necessary to ensure optimum signal demodulation. The control unit is responsible for switching between training sequence and decision-directed adaptation. A block responsible for bit synchronization can be included here.

The control unit may also incorporate a correlator which correlates the input with the known spreading code multiplied by the estimated symbols as a means of verifying the symbol estimates. Correlating over several symbols has the advantage of rejecting more noise than correlating over a single symbol interval.

1. For initial signal detection, the receiver correlates the incoming signal with a "wake up" sequence. The sum of the squared inphase and quadrature outputs of the correlator is used to decide whether a transmitter is trying to reach the receiver. Since the correlator correlates over a length of several bits, a high peak value can be observed at its output. After sending the initial sequence, the transmitter sends a training

sequence to facilitate convergence of the RLS algorithm.

2. During training, the complex correlator correlates the input with the spreading code multiplied by the corresponding training symbols. The sum of the squared inphase and quadrature components of the correlator's output is used for bit synchronization. The phase between the inphase and quadrature components is used for carrier phase locking.

3. In demodulation mode, the correlator correlates the received signal with a sequence generated by the spreading code and the last symbols estimated by the receiver to verify proper operation of the unit and to maintain bit and carrier synchronization.

In addition to the above mentioned implementation, the control unit can also incorporate error-correction coding. A system clock connected to each block allows synchronous operation among the receiver components. Finally, the estimated data is available at the output of the buffer.

4.5 Multipath Propagation and Fading

In a real system, the effects of the channel need to be considered. In a mobile system, the channel is characterized by frequency-selective and time-selective fading. A transmitted signal is distorted by multipath propagation and Doppler-shifts. Multipath propagation results from reflections from buildings and natural obstacles. The velocity of a vehicle introduces a frequency-shift. It depends on the angle of arrival of the received waveform. Since multipath components might arrive from different directions, each multipath component experiences a different frequency shift. This section discusses how the receiver can compensate for multipath propagation and fading.

Multipath propagation can be mitigated by the receiver in the same way that an equalizer mitigates multipath. The filter needs to be sufficiently long to compensate for the multipath. However, it should be mentioned that increasing the size of the tapped delay line decreases the convergence rate of the RLS algorithm and increases its computational costs. Multipath components can be exploited by the algorithm as long as they are fading slow enough to be tracked. Otherwise, these components must be viewed as interference.

The fading nature of the mobile channel introduces severe problems for the detection and interference rejection of the desired signals. In many of these cases, the receiver has to rely on tracking capabilities of the coefficient update algorithm. For fast time-varying channels, the ability to find the optimum weighting vector must be traded for tracking capabilities.

A more detailed analysis of the impact of fading on the performance is a future research topic.

Chapter 5

Performance of the Receiver

In Chapters 3 and 4 it is shown that if the spreading codes repeat at the bit rate and an adaptation algorithm is used constantly to adapt the weights of a vector used for despreading and demodulation, substantial performance gains over conventional receivers can be expected when MAI is present. Adaptation of the weight vector is executed at the bit rate and real arithmetic is preferred. To demonstrate the superior performance, various scenarios are simulated. These scenarios are discussed in this chapter.

5.1 Simulation Model

Devices employing DS-SS signaling schemes are proposed for the mobile channel. Reasons for employing a DS-SS signaling scheme are given in Section 1.1. For testing the performance of a certain system design using simulations, the effects of the channel need to be considered [27, 28]. The mobile channel is one of the most problematic channels. It can be characterized by its time-varying and frequency-selective fading nature. In addition, a transmitted signal can be time-displaced and/or Doppler-shifted. Doppler-shifts result from the velocity of the mobile or objects in the channel. The velocity, v, the wavelength of the signals, λ, and the angle of arrival determine the amount by which the signal is shifted in frequency. In particular, the Doppler frequency, f_D, is given by

$$f_D = \frac{v}{\lambda} \cos \gamma, \tag{110}$$

where γ denotes the angle of arrival as pictured in Figure 20. If multipath propagation is encountered, each path might inherit its own Doppler frequency depending on its angle of arrival. Also, depending on its origin, each multipath component may have different fading statistics [29]. Modeling a realistic mobile channel is very expensive and requires a great
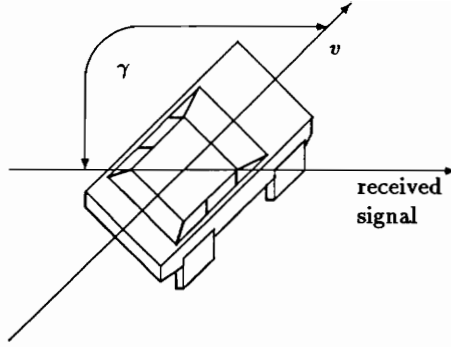
Figure 20: Angle of arrival.

amount of computational costs. For modeling a mobile channel, the reader is referred to the literature, e.g., [30, 31].

In this thesis, however, the channel model is simplified to ease the simulations. The main simplification of the channel modeling lies in assuming that the channel characteristics are varying slowly enough such that the channel can be assumed static for a short block of data. The impact of the time-varying nature of the channel on the deviation in between a bit sequence depends on the bit rate. This impact might be mitigated (to a certain extent) by choosing a higher bit rate.

Another major simplification in the simulation models is that only one frequency shift per user, i.e., the angle γ in Equation 110 is the same constant for all multipath components attributed to a user. However, frequency-shifts model the tolerances among the oscillators for all users.

Making these assumptions, the simulation model used for all simulations in this thesis can be represented by the diagram illustrated in Figure 21. For each user i, the data bits are multiplied by the spreading sequence. The parameter τ_i is a random delay of which the ith user is transmitting its symbols. Since it is assumed that the conversion to baseband has already taken place at the receiver, each product is further multiplied by a complex carrier $A_i e^{j\omega_i t + \varphi_i}$ with $\omega_i = 2\pi f_i$, where f_i represents the sum of the deviations caused by the transmitter oscillator imperfections and Doppler effects, and A_i^2 is the transmitted power of the ith user. The constant φ_i denotes an initial phase-offset for each user. Each user's signal is convolved with a different channel response $h_i(t)$. The receiver sees the sum of all distorted signals plus noise, $n(t)$.

Even though the model of the mobile channel is simplified, the simulation model in Figure 21 gives insight into the behavior of the proposed receiver compared to conventional
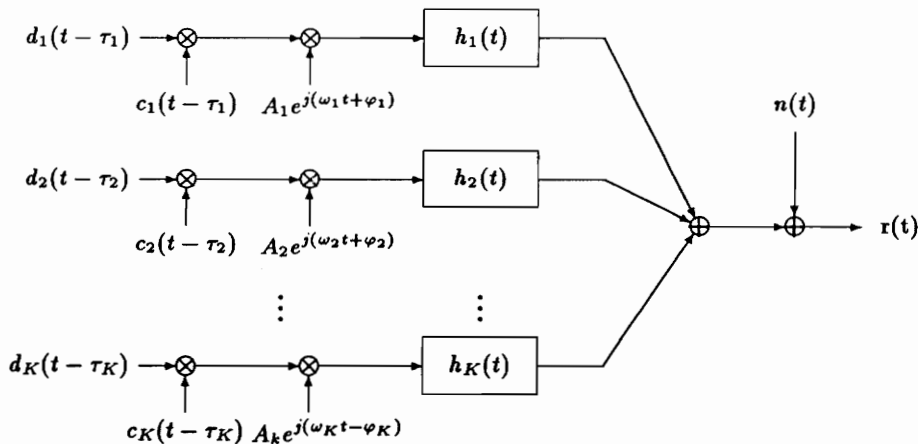
Figure 21: System model.

techniques.

5.2 Performance of the Receiver in the AWGN Channel

This section is devoted to evaluating the performance of the receiver in the presence of *additive white Gaussian noise* (AWGN) and multiple access interference. The AWGN channel is the simplest channel involving no multipath components. It is assumed that the signals for each user propagate undistorted through the channels, $h_i(t)$. Only white Gaussian noise is added to the signals. Hence, the impulse response $h_i(t)$ is

$$h_i(t) = \delta(t), \tag{111}$$

where $\delta(t)$ is the unit impulse response or Dirac delta function. The noise variable $n(t)$ can be described by

$$n(t) = n_r(t) + jn_i(t), \tag{112}$$

where $n_r(t)$ and $n_i(t)$ are two independent zero-mean Gaussian random variables with uniform power spectral density.

In simulating the AWGN channel for multiple users, despread SNRs of 10, 15, 20, and 25 dB are considered.[1] Since many applications for CDMA DS/SS are cellular voice transmission systems, the bit rate R_b is set to 16.384 kbit/s. This bit rate is reasonable, since modern vocoders operate at bit rates of 9600 bit/s and below [32]. A set of spreading codes

---

[1]The despread SNR is the SNR which is seen at the receiver after despreading and low-pass filtering a DS-SS signal.

Table 2: Simulation Parameters

Processing gain . . . . :	31
Sampling factor . . . . :	2
Bit rate . . . . :	16.384 kHz
Chip rate . . . . :	507.904 kHz
Sampling rate . . . . :	1015.808 kHz
Frequency standard deviation:	500 Hz
Power standard deviation . . . . :	1 dB

with low cross- and autocorrelation properties are used for the simulations. As discussed in Section 4.4.3, the sampling rate is set to an integer multiple of the bit rate but no lower than twice the processing gain. For these simulations, the sampling rate is set to the minimum value of twice the bit rate times the processing gain, i.e. $f_s = 1,015.808$ kHz. Since perfect power control cannot be achieved in real-world systems, the simulation model allows different power levels between the users. In this model, it is assumed that the deviation of the power levels of the users is normal distributed on a dB scale. In the most common set-up, the standard deviation of the power levels is set to 1 dB. Another parameter is the frequency offsets, f_i, introduced by carrier tolerances and Doppler-shifts as described in Section 5.1. For modeling these offsets, it is assumed that the received frequencies deviate from a desired frequency with a normal distribution. Since the signal is processed at baseband, f_i is a zero-mean Gaussian variable. Its standard deviation is set to 500 Hz. Table 2 summarizes the parameters for the simulations described in this section.

In Figure 22 a typical simulation scenario is depicted for $K = 25$ users. It shows the initial phases, φ_i, for all users. The phases are random and uniformly distributed over the interval $[0, 2\pi)$. Also shown are the different amplitude levels, A_i, and the different relative frequencies.

The term "sample offset" needs some further explanation; the simulation model is a discrete-time model, so the time-delays, τ_i, seen by the receiver take on discrete values. In particular, each discrete delay is an integer multiple of the sampling period $1/f_s$. Hence, each user's signal is shifted by an integer number of samples. Since all bits are randomly produced and are statistically independent and since the bit period corresponds to 64 samples, without loss of generality, these shifts can be limited from 0 to 63 samples. The figure shows the deviation of the sample offsets of all users from the mean value.

In all simulations, the updating of the weighting vector, $\mathbf{w}[n]$, is performed using the RLS algorithm as described in Section 4.4.

As discussed in Section 4.4.2, in some cases a weighting function, $\Psi(x)$, which weights
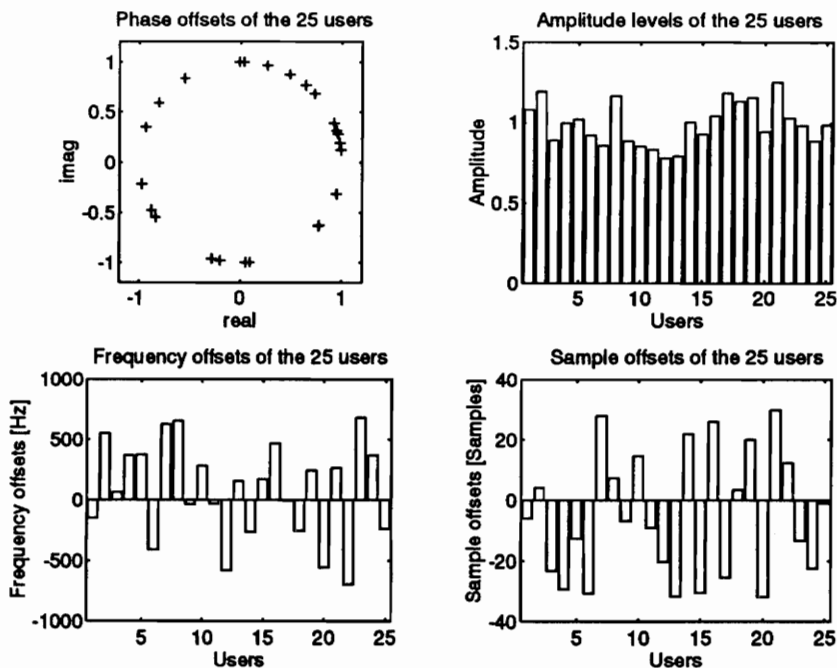
Figure 22: Scenario for 25 users.

the correction of the vector $w[n-1]$ depending on the likelihood of the correctness of the update is applied. Two cases are investigated:

1. In the first case, the likelihood of correct decision is not taken into account. Therefore, $\Psi(x) = 1$ for all symbols.

2. In the second case, a weighting function is employed. For BPSK signaling, symbols from the set $\{-1, 1\}$ are used. If the absolute value of $\hat{d}[n]$ is less than 0.5, then the algorithm does not update the weighting vector. In all other cases, the updating proceeds without any modifications, i.e., $\Psi(x) = 1$.

5.2.1 Simulations Using No Weighting Function

Figures 23 through 26 show the performance of the optimum single user detector for *signal-to-white-noise ratios*[2] (SWNRs) of 10, 15, 20, and 25 dB, respectively. In these simulations, the first case of the weighting vector update function is applied. The figures also show the theoretical BER performance curve for the matched filter as given by Holtzman [7].[3] In the

---

[2]Here, the SWNR is the ratio of the energy of one single user to the channel noise energy after despreading.
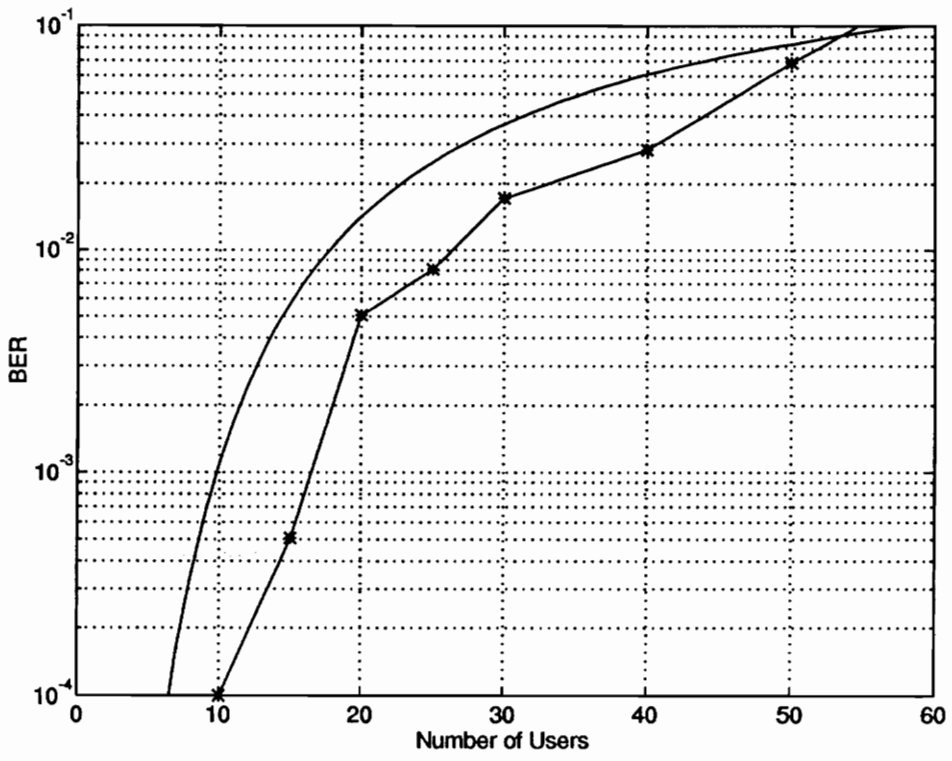[3]See also Section 2.1.2.

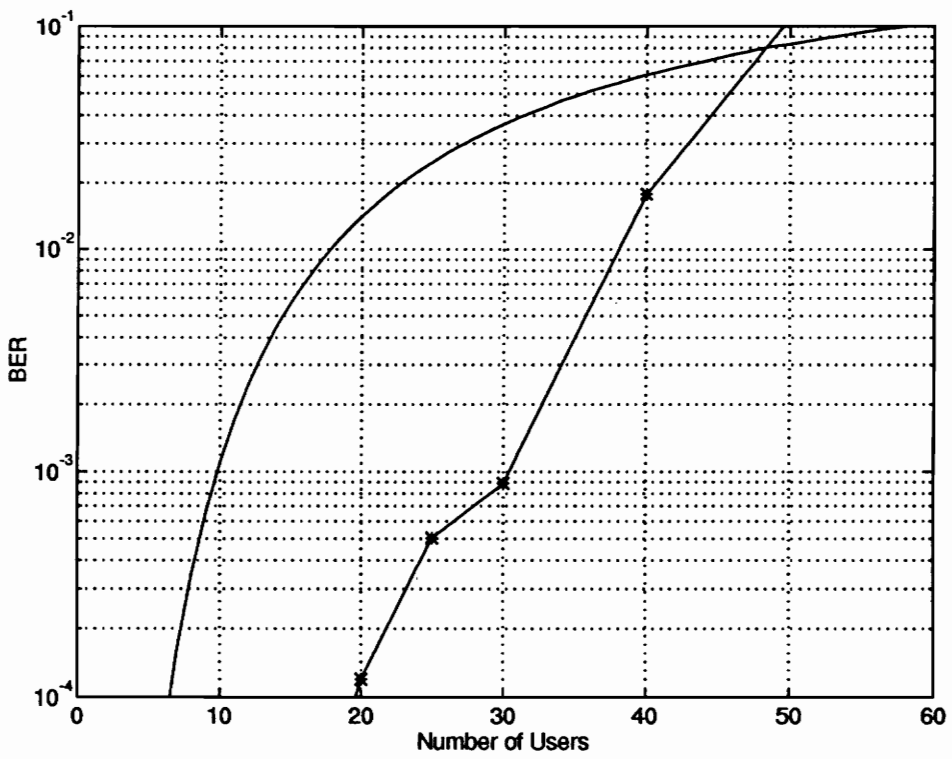Figure 23: Performance of the receiver for 10 dB SWNR.

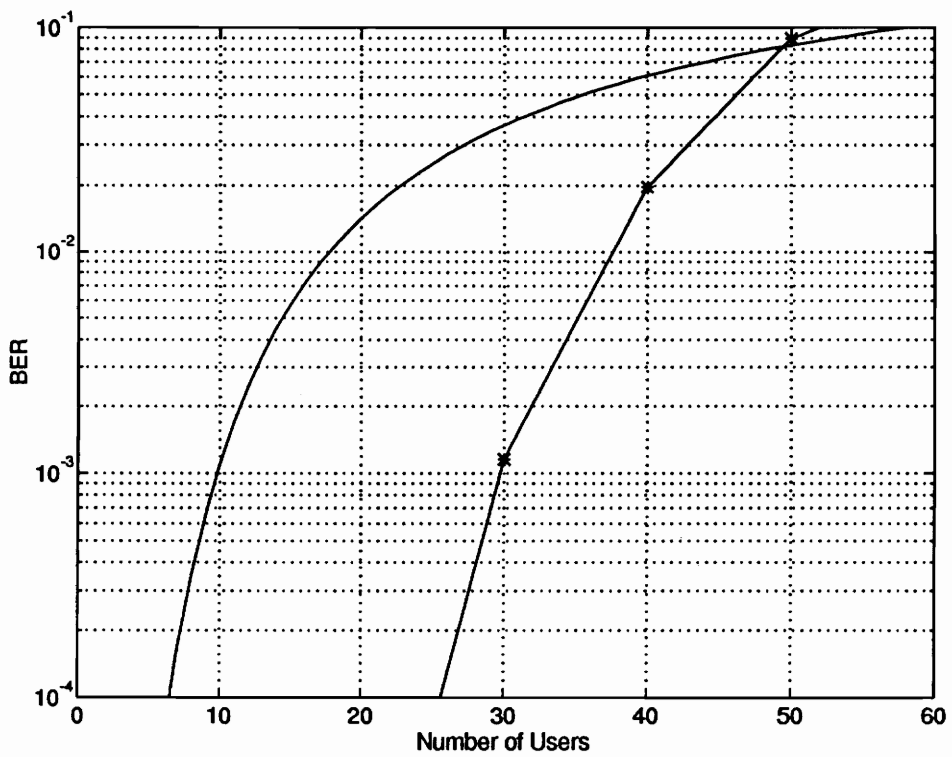Figure 24: Performance of the receiver for 15 dB SWNR.
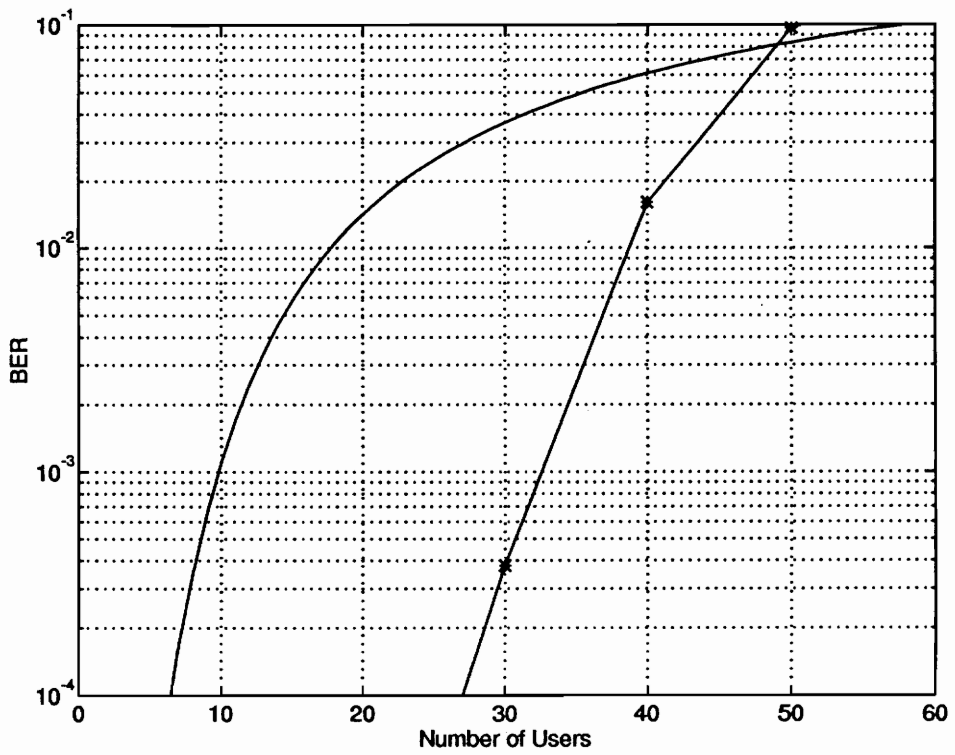
Figure 25: Performance of the receiver for 20 dB SWNR.

Figure 26: Performance of the receiver for 25 dB SWNR.

simulations, the first 300 bits are used for training. After training is complete, the receiver is switched to decision-directed mode. From Figure 23, it can be seen that the performance of the receiver is only slightly better than of the matched filter receiver with fixed weights. The low SWNR increases the weight convergence time. The SNR for the desired signal is too low for good BER performance. Still, the BER is roughly 50 percent lower than the BER of the correlation receiver.

As the SWNR increases, tremendous improvements over the conventional receiver can be obtained. This can be seen from Figures 24, 25 and 26. For all three cases, the system supports 30 users at a BER of 10^{-3}. Note that this is almost ideal FDMA capacity. Furthermore, it can be seen that the BER for a lower number of users is lower for 20 and 25 dB SWNR than for the case of 15 dB SWNR. The performance of the correlation receiver remains almost the same, since it primarily suffers from the impact of the MAI. As the number of users exceeds the processing gain, the performance of the optimum single-user detector approximates the performance of the correlation receiver. For $K = 50$ users, the receiver's performance is worse. This behavior follows from the set-up of the coefficient update algorithm. In this case, too many false decisions keep the weight vector from converging to a meaningful solution. Hence, it experiences the case of a catastrophic failure. For a high number of users the BER approaches 50 percent.

5.2.2 Simulations Employing a Weighting Function

In the second case, a weighting function $\Psi(x)$ is employed for the simulations. In particular, $\Psi(x)$ is set to

$$\Psi(x) = \begin{cases} 0 & |x| < 0.5 \\ 1 & |x| \geq 0.5 \end{cases} \tag{113}$$

Employing such a function, the catastrophic failure rate is reduced. The only bits used for adaptation are those with a high likelihood of correctness.

Figures 27 through 30 show the performance of the optimum single user detector for SWNRs of 10, 15, 20, and 25 dB, respectively. Like Figures 23 through 26, the figures also show the theoretical BER performance curve for the matched filter as given by Holtzman. Likewise, the first 300 bits are used for training. After training, the receiver is switched to decision-directed mode.

It can be seen that the receiver with the weighting function shows the same characteristics as for the case presented in Section 5.2.1. Referring to Figure 27, for a low SWNR, the receiver shows only a slight increase of performance over the conventional receiver. The energy of the SOI is not sufficient to provide good decisions.
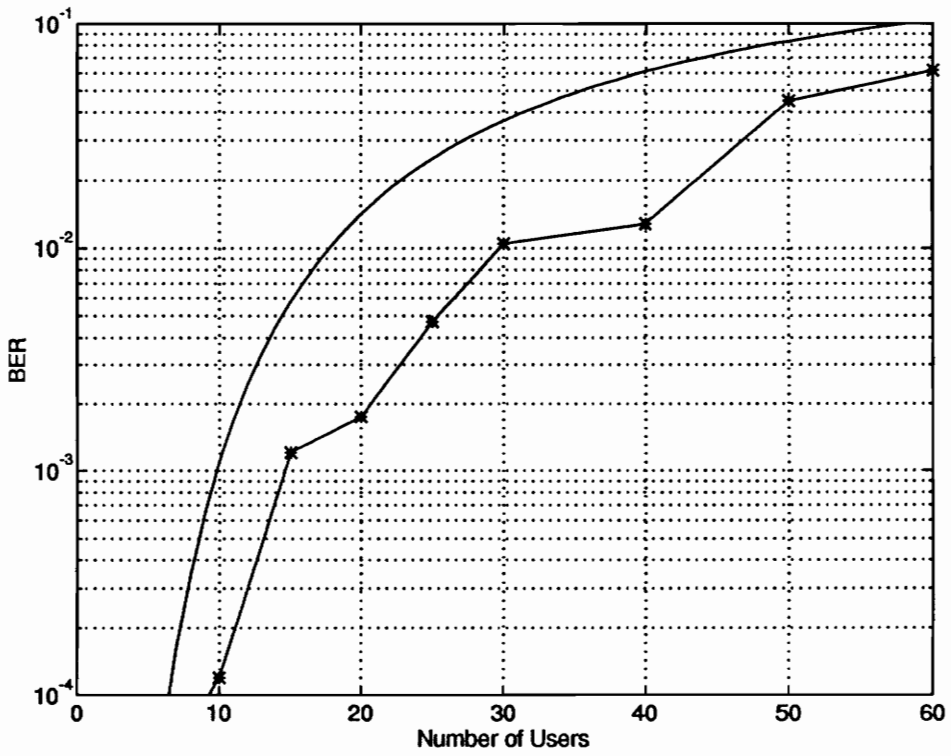
47

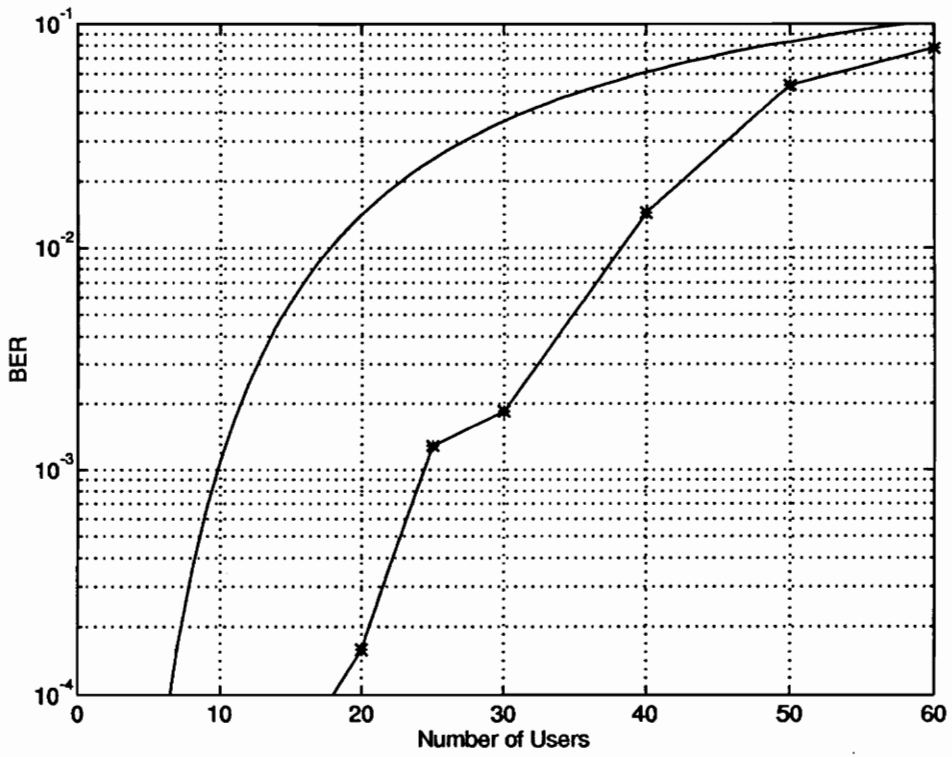Figure 27: Performance of the receiver for 10 dB SWNR.

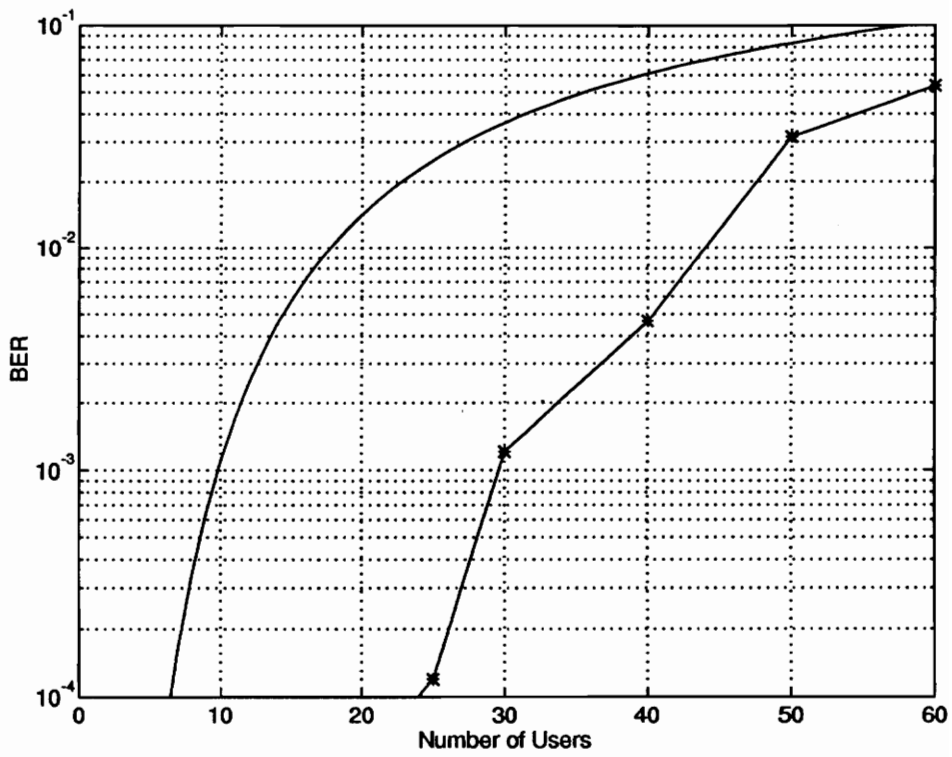Figure 28: Performance of the receiver for 15 dB SWNR.

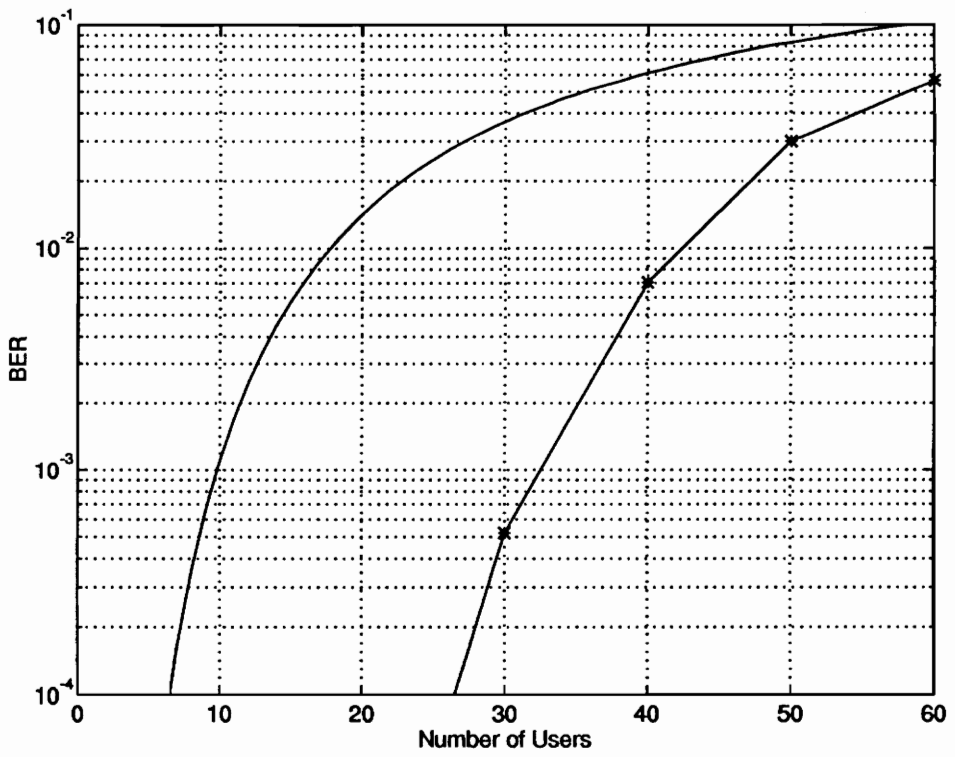Figure 29: Performance of the receiver for 20 dB SWNR.

Figure 30: Performance of the receiver for 25 dB SWNR.

As the SWNR becomes higher, the performance over the conventional receiver increases. This is seen in Figures 28, 29 and 30. However, major differences can be noticed by comparing Figures 23 to 26 to Figures 27 to 30. The receiver employing the weighting function described by Equation 113 performs worse for the range of ten to thirty users. For the number of users exceeding the processing gain (or ideal FDMA capacity), the receiver using the weighting function performs better. In fact, even for $K = 60$ users, the receiver still performs better than the conventional receiver. This is expected, since the weighting function $\Psi(x)$ inhibits the RLS algorithm from updating on false decisions. However, for ten to thirty users the likelihood of making a wrong decision is low enough so continuously updating the weight vector helps to increase the performance as shown in Figures 23 to 26.

The choice of the weighting function depends on the demands placed on the system. Also, the characteristics of the receiver depend on the nature of the channel and on the noise function, $n(t)$.

5.3 Real Versus Complex Arithmetic

Justification for using real arithmetic over complex arithmetic is given in Section 4.2. This section is devoted to demonstrating the benefits of real arithmetic over complex arithmetic for the optimum linear single user detector.

In this set of simulations, a BPSK DS-SS signal applying the same simulation model as in Section 5.2 is employed. Its system parameters are given in Table 2.

Figure 31 shows the constellation diagram for a BPSK DS-SS signal for one particular user after despreading. The total number of users is $K = 30$ and the SWNR is 15 dB. In this case, the weighting vector, $\mathbf{w}$, is found by solving the normal equations for a complex $d[n]$, hence, it minimizes the MSE measured with respect to both the real and imaginary part of the error. The figure shows two clusters of the noisy estimates, $\hat{d}[n]$, centered at $-1 + j0$ and $+1 + j0$. Although the MSE is minimized, the separation of the clusters is not sufficient to allow a clear classification for some $\hat{d}[n]$ which lie close to the imaginary axis. In fact, for 2300 bits, there are more than twenty errors.

As discussed in Section 4.2, it is more meaningful to minimize the MSE for the real part only. Figure 32 illustrates the constellation diagram for the same signal and user using the real part only in the error-criterion. Since no constraints is imposed on the imaginary part of the estimates, $\hat{d}[n]$, the clusters are much more spread out along the imaginary axis than for the case of Figure 31. However, the clusters are better centered along the real axis and a clear classification of the estimates $\hat{d}[n]$ is possible. In fact, using this technique, no false decisions are made.
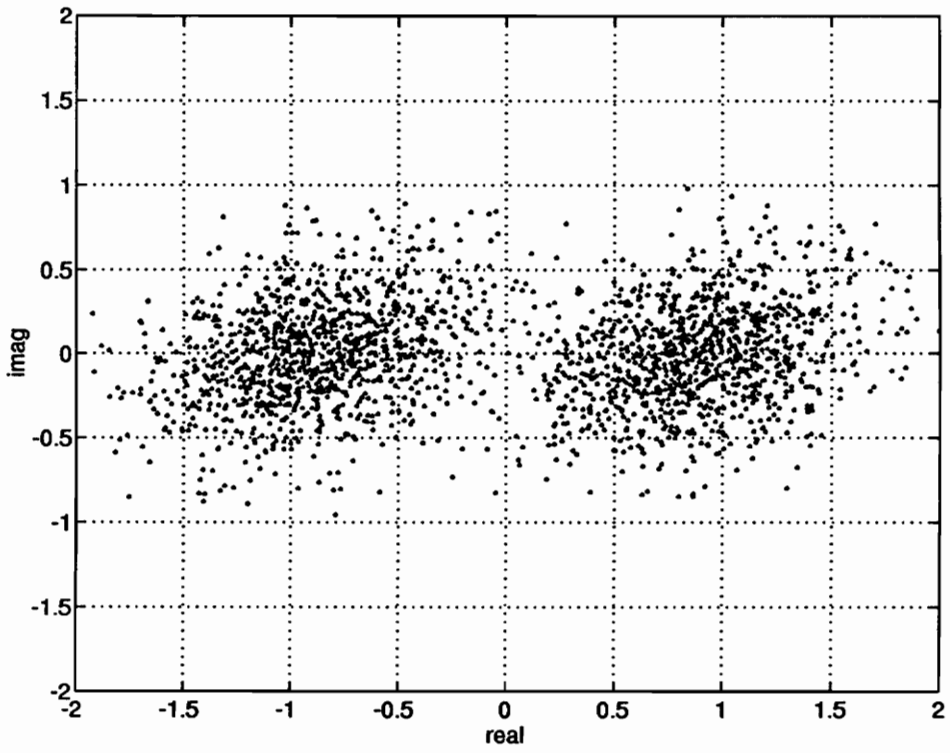
52

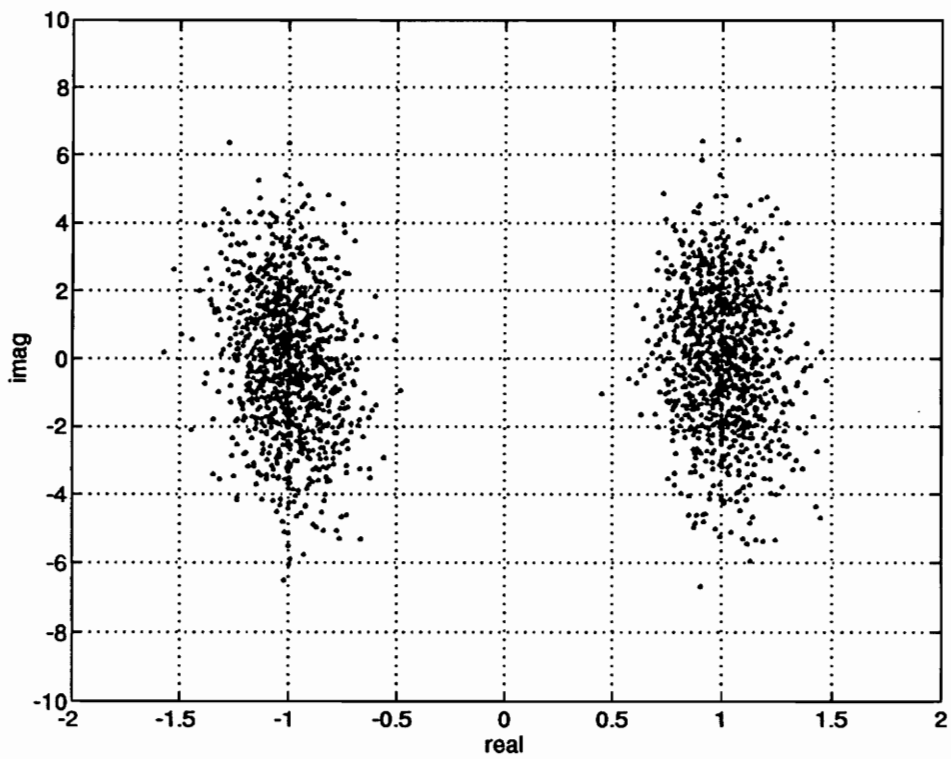Figure 31: BPSK constellation diagram after despreading using complex arithmetic.

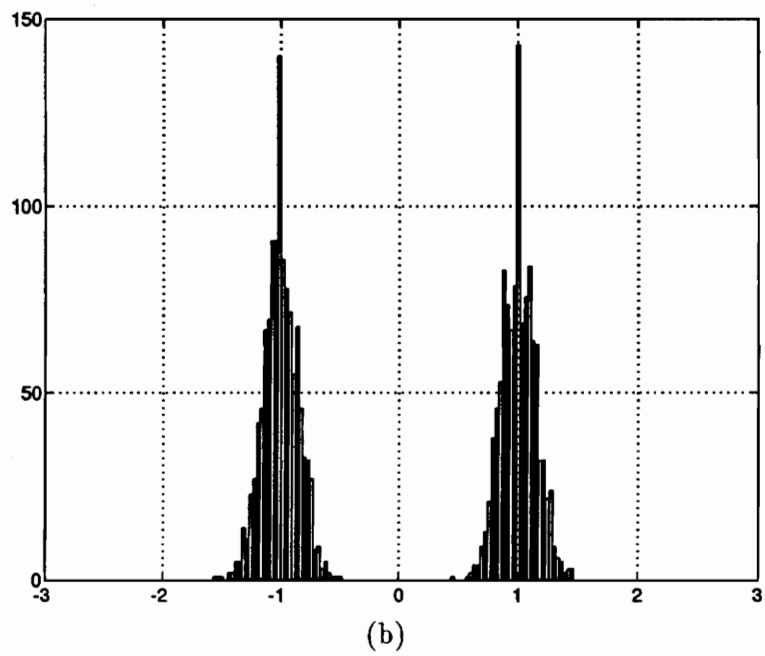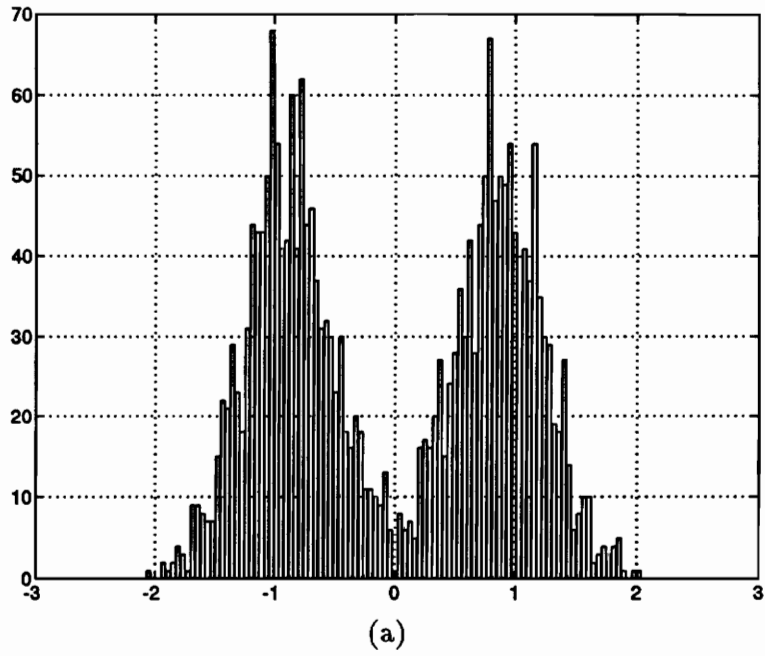Figure 32: BPSK constellation diagram after despreading using real arithmetic.

Figure 33: Histogram for the real part for (a) complex and (b) real arithmetic.

Processing gain . . . . :	31
Sampling factor . . . . :	2
Bit rate . . . . :	262.144 kHz
Chip rate . . . . :	8.126464 MHz
Sampling rate . . . . :	16.252928 MHz
Frequency standard deviation:	500 Hz
Power standard deviation . . . . :	1 dB

Figure 33a illustrates the histogram for the real part of the signal shown in Figure 31. Figure 33b shows the histogram for the real part of the signal shown in Figure 32 for which the data is much better centered around the desired signal points.

Obviously, minimizing the error in the real component is preferable to minimizing the complex error to obtain a lower BER.

5.4 Characteristics of the Receiver in a Multipath Environment

In this section, results obtained from simulations of the optimum single user detector for multipath channels are presented. The bit rate is increased to emphasize the multipath effects. The bit rate is increased by a factor of 16, i.e., a bit rate of 262.144 kbit/s is assumed. Thus, the bit duration is 3.81 μs. Table 3 gives an overview of the parameters used in these simulations.

For the multipath propagation a one-sided exponential delay power profile, $p_\tau(\tau)$, is assumed [33, 34]. In these simulations, the delay power profile is set to

$$p_\tau(\tau) = \begin{cases} e^{-\tau/b}, & 0 \leq \tau \leq 2 \ \mu s, \\ 0, & \text{otherwise}, \end{cases} \tag{114}$$

where $b = 1$ μs. Figure 34 shows a graphical representation of $p_\tau(\tau)$.

The model assumes five paths, in which the path delays, $\tau_{i,p}$, $1 \leq p \leq 5$ are uniformly distributed within the ranges listed in Table 4. One sample delay corresponds to a delay interval of 61.52 ns. It is assumed that the amplitudes in each path are Rayleigh distributed. The phase for each path is uniformly distributed. Figure 35 depicts the channel impulse responses for the first 10 users.

For these simulations a SWNR of 25 dB is assumed. The length of the tapped delay line is adjusted to match the length of the observed symbols. In particular, the length is set

Figure 34: Delay power profile.
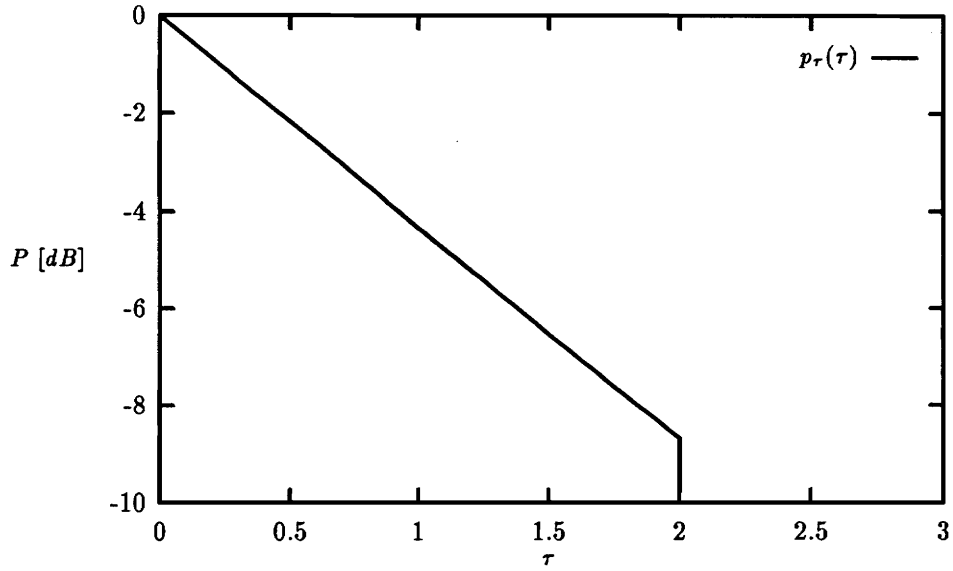
Table 4: Distribution of the sample delays

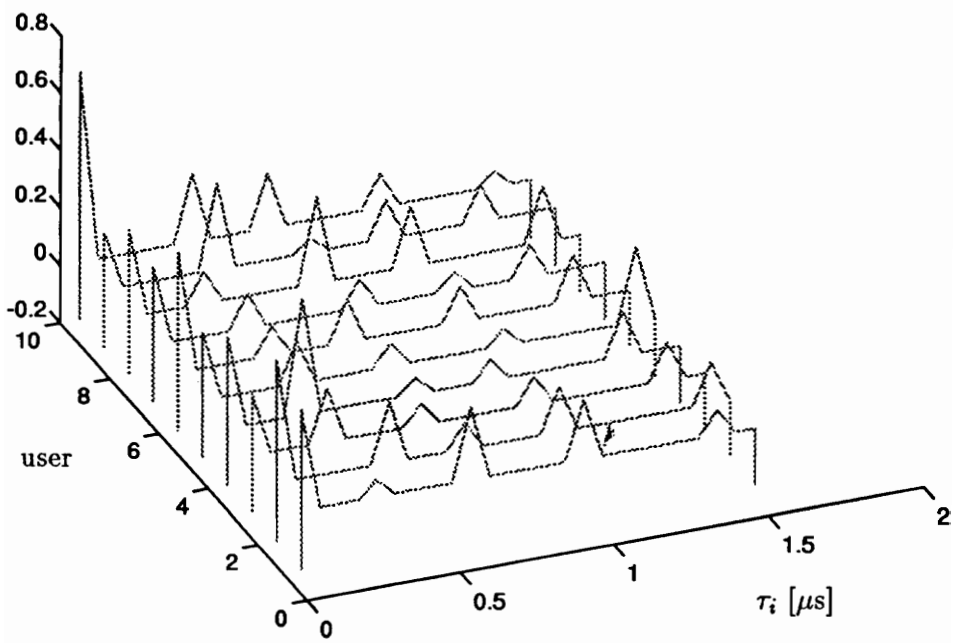| path p	min	max
	samples	
1	1	1
2	5	7
3	10	12
4	15	17
5	20	25

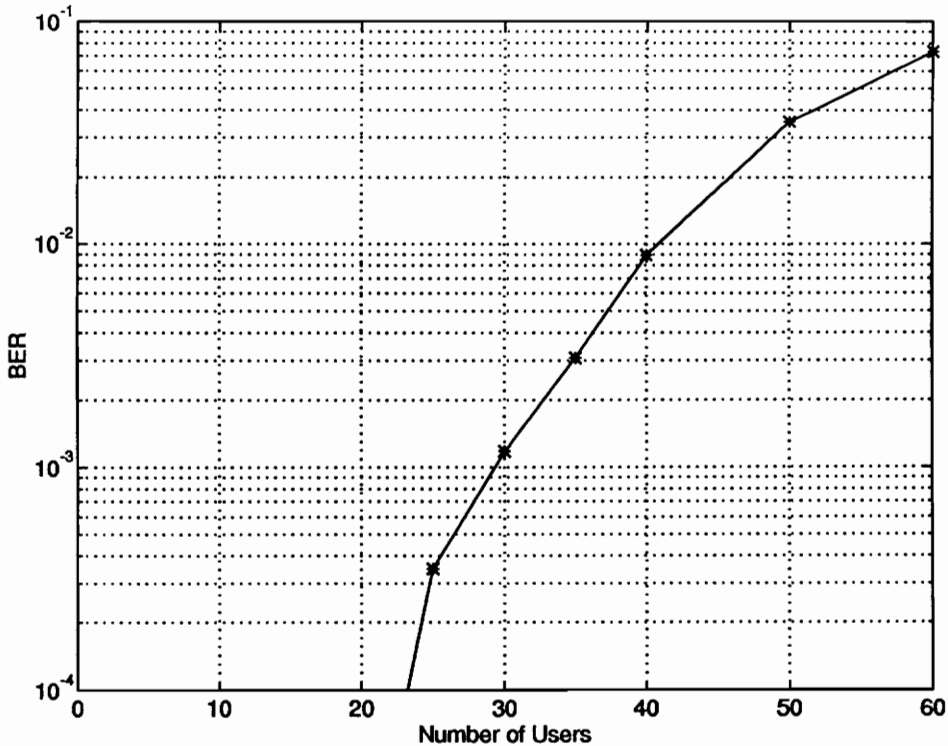Figure 35: Channel impulse responses for the first 10 users.

Figure 36: Performance of the optimum single user detector for multipath channels.

to hold 90 complex or 180 real samples. This equals a duration of approximately 5.54 μs and is 1.72 μs more than the bit period. A total of 300 bits are used for training. Also, the rectangular weighting function $\Psi(x)$ given by Equation 113 is applied.

The results of the simulations are presented in Figure 36. It can be seen that, even though the received signal is heavily distorted by the multipath, the receiver is still able to produce good results. Comparing the performance of the multipath channel simulations to the AWGN channel for the same SWNR (Figure 30), it can be concluded that the receiver performance is only slightly worse for the multipath channel. Simulating the performance of the receiver in all different environments should be included in future performance evaluations (see also Section 6.2).
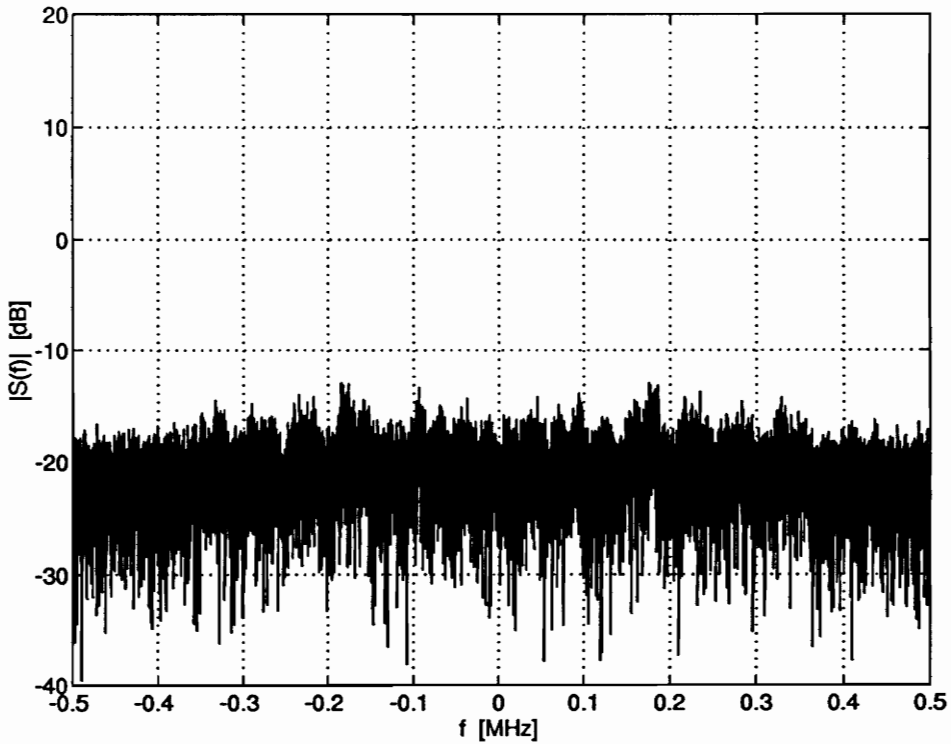
Figure 37: Magnitude spectrum of a single user.

5.5   Narrowband Interference Cancellation

The receiver is also capable of rejecting narrowband interference by adaptively configuring a notched filter.

This principle is demonstrated by simulations. Figure 37 illustrates the *magnitude spectrum* of a single CDMA user having the same parameters as tabulated in Table 2 corrupted by white Gaussian noise. In Figure 38 the same signal, corrupted by five narrowband interferers having a 20 dB higher signal power than the SOI, is shown. Simulations showed that the receiver is able to demodulate the SOI without making errors while a matched filter produces 50 percent BER.[4]

---

[4]In this simulation, only 20,000 bits are used. The BER is expected to be less than 5×10^{-4}.
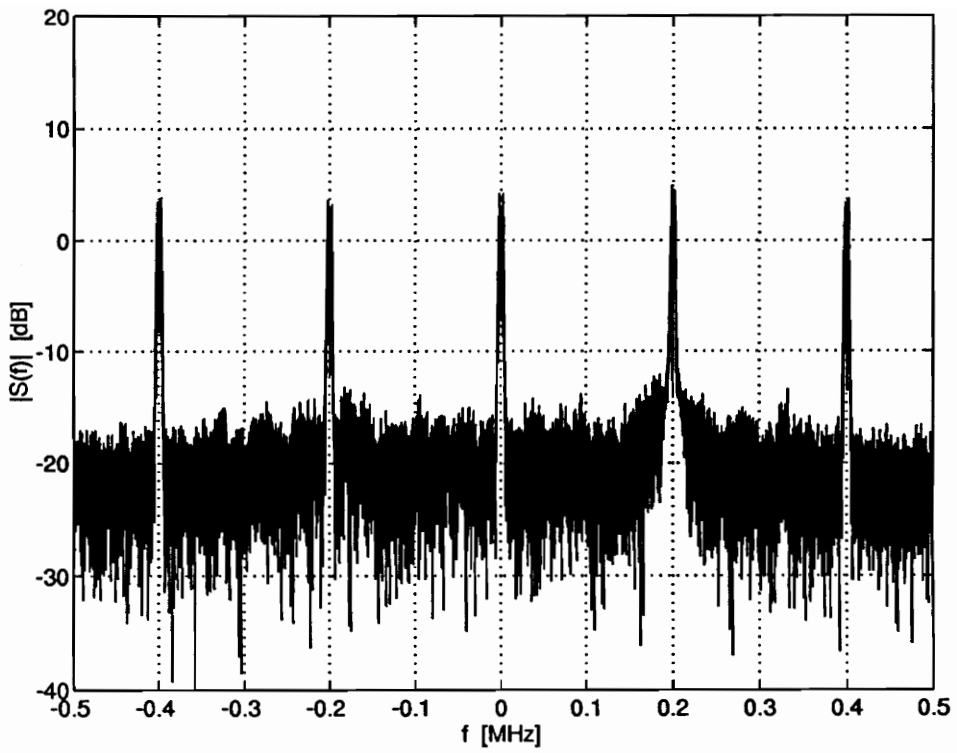
Figure 38: Magnitude spectrum of a single user and five narrowband interferers.

Chapter 6

Conclusions and Future Work

In this thesis, a different approach to demodulating a CDMA DS-SS signal is demonstrated. It is shown that if code-on-pulse modulation is used to spread a signal, then the repetitive nature of the signal and the interference can be used to find a filter which has a lower BER than the conventional correlation receiver. In this case, the linear filter which is optimized for demodulating the signal is the optimum time-dependent adaptive filter for exploiting the cyclostationarity in the signal of interest and the multiple access interference. Chapter 5 shows tremendous improvements for the performance of a code-on-pulse CDMA receiver over the conventional correlation receiver. These gains are achieved without any knowledge of the interference. Solely, the spectral correlation in the signal of interest and the interference is exploited.

Furthermore, it is shown that, to allow maximum performance of a receiver in a BPSK DS-SS CDMA system, the normal equations are best solved to minimize the MSE along the real axis. Since the imaginary part is not considered for symbol decision, this allows for an additional degree of freedom to minimize the error in the real part. The error along the real axis is more reflective of the BER than the error for both the real and imaginary parts.

The computational complexity of the proposed receiver is approximately that of the conventional equalizer.

6.1 Potential Drawbacks

Throughout the simulations presented in Chapter 5, a static channel model is assumed. Since the environment constantly changes, the coefficient update algorithm must change the weight vector continuously in order to keep the weight vector at its optimum value. The ability to rapidly adapt to a dynamic channel has yet to be proven. In Sections 4.5

and 5.4, it is shown that the receiver is still able to produce good results, even if the signals experience multipath distortion.

The exponentially weighted RLS algorithm presented in Section 4.4.1 is best suited for handling the time-varying environment. However, its biggest shortcoming is the need for an inverse correlation matrix. Computations increase with the square of the length of the tapped delay line. In a mobile system, where battery life and costs are the principal constraints on the design of the mobile receiver, this implementation might not be suitable.

6.2 Future Research

The system presented is a desirable alternative to CDMA systems employing long pseudo-random codes to spread their signals. The receiver structure allows low cost implementation and requires no *a priori* knowledge about multiple-access interferers. Substantial performance gains are obtained in the simulations shown in Chapter 5. To allow an evaluation of the performance in realistic channels, future research should include simulations for various types of channels using more exact channel modeling. Furthermore, it is desirable to develop formulas to give a theoretic approximation of the new receiver's BER performance.

It is shown in Section 4.2 that it is desirable to decouple the normal equation for the real and imaginary part. Comparisons between the receivers applying this technique and receivers which minimize the conventional MSE should be investigated in the future.

Bibliography

[1] D. R. Hush and B. G. Horne, "Progress in supervised neural networks," *IEEE Signal Processing Magazine*, Jan. 1993.

[2] P. Jung, P. W. Baier, and A. Steil, "Advantages of CDMA and spread spectrum techniques over FDMA and TDMA in cellular mobile radio applications," *IEEE Transactions on Vehicular Technology*, vol. 42, no. 3, pp. 357–364, Aug. 1993.

[3] Committee on Digital CDMA Cellular, "IS-95 wideband spread spectrum digital cellular system dual-mode mobile station — base station compatibility standard," tech. rep., EIA/TIA, TR45.5, Apr. 1992.

[4] R. L. Pickholtz, D. L. Schilling, and L. B. Milstein, "Theory of spread-spectrum communication — a tutorial," *IEEE Transactions on Communications*, vol. COM-30, pp. 855–884, May 1982.

[5] A. V. Oppenheim and R. W. Schafer, *Discrete-Time Signal Processing*. Prentice Hall, 1989.

[6] L. W. Couch, *Digital and Analog Communication Systems*. New York: Macmillian Publishing Company, third ed., 1990.

[7] J. M. Holtzman, "A simple accurate method to calculate spread spectrum multiple access error probabilities," *ICC 91 Conference Record*, vol. 3 of *3*, (Denver), pp. 1633–1636, IEEE Communication Society and the Denver IEEE Section, June 1991.

[8] R. K. Morrow, Jr. and J. S. Lehnert, "Bit-to-bit error dependence in slotted DS/SSMA packet systems with random signature sequences," *IEEE Transactions on Communications*, pp. 1052–1061, Oct. 1989.

[9] G. D. Forney, "The Viterbi algorithm," *Proceedings of the IEEE*, vol. 61, pp. 268–278, Mar. 1973.

[10] S. Verdú, "Minimum probability of error for asynchronous gaussian multiple-access channel," *IEEE Transactions on Information Theory*, vol. IT-32, no. 5, pp. 642–651, Sept. 1986.

[11] S. Verdú, "Computational complexity of optimum multiuser detection," *Algorithmica*, vol. 4, no. 3, (New York), pp. 303–312, Springer-Verlag, 1989.

[12] B. Aazhang, B.-P. Paris, and G. C. Orsak, "Neural networks for multiuser detection in code-division multiple-access communications," *IEEE Transactions on Communications*, vol. 7, no. 40, July 1992.

[13] M. K. Varansi and B. Aazhang, "Multistage detection for asynchronous code-division multiple-access communications," *IEEE Transactions on Communications*, vol. 38, pp. 509–519, Apr. 1990.

[14] B. G. Agee, "Solving the near-far problem: Exploitation of spatial and spectral diversity in wireless personal communications networks," *Proceedings of the Third Annual Symposium on Wireless Communications*, vol. 1, pp. 15–1,15–12, Virgina Polytechnic Institute and State University, Mobile and Portable Radio Research Group, June 1993.

[15] W. A. Gardner, "Spectral correlation of modulated signals: Part I — analog modulation," *IEEE Transactions on Communications*, vol. COM-35, no. 6, pp. 584–594, June 1987.

[16] W. A. Gardner, W. A. Brown III, and C.-K. Chen, "Spectral correlation of modulated signals: Part II — digital modulation," *IEEE Transactions on Communications*, vol. COM-35, no. 6, pp. 595–601, June 1987.

[17] W. A. Gardner, *Statistical Spectral Analysis: A Nonprobabilistic Theory*. Englewood Cliffs: Prentice-Hall, 1987.

[18] R. D. Holley, "Time dependent adaptive filters for interference cancellation in CDMA systems," Master's Thesis, Virginia Polytechnic Institute and State University, Oct. 1993.

[19] C.-K. Chen, *Spectral Correlation Characterization of Modulated Signals with Application to Signal Detection and Source Location*. Ph.D. Dissertation, Department of Electrical and Computer Engineering, University of California at Davis, 1988.

[20] W. A. Gardner, "Cyclic Wiener filtering: Theory and method," *IEEE Transactions on Communications*, vol. 41, no. 1, pp. 151–163, Jan. 1993.

[21] J. H. Reed, *Time Dependent Adaptive Filters for Interference Rejection.* Ph.D. Dissertation, Department of Electrical and Computer Engineering, University of California at Davis, Dec. 1987.

[22] J. H. Reed and T. C. Hsia, "The performance of time-dependent adaptive filters for interference rejection," *IEEE Transactions on Acoustics, Speech, and Signal Processing,* vol. 38, no. 8, Aug. 1990.

[23] J. H. Reed, C. D. Greene, and T. C. Hsia, "Demodulation of a direct sequence spread-spectrum signal using an optimal time-dependent receiver," *1989 IEEE Military Communication Conference,* pp. 37.6.1–37.6.4, Oct. 1989.

[24] S. Haykin, *Adaptive Filter Theory.* Englewood Cliffs, New Jersey: Prentice-Hall Publishing, first ed., 1986.

[25] S. Haykin, *Adaptive Filter Theory,* pp. 447–506. Prentice-Hall, Inc., second ed., 1991.

[26] W. Huang and T. Rappaport, "A comparitive study of two adaptive equalizers for mobile radio," *Proceedings of the 1991 IEEE Vehicular Technology Conference,* pp. 765–769, IEEE Vehicular Technology Society, May 1991.

[27] T. S. Rappaport, S. Y. Seidel, and R. Singh, "900 MHz multipath propagation measurements for US digital cellular radiotelephone," *IEEE Global Telecommunications Conference and Exhibition,* vol. 1 of *3,* pp. 84–89, Nov. 1989.

[28] A. B. Johnson, "Simulation of digital transmission over mobile channels at 300 kb/s," *IEEE Transactions on Communications,* vol. 39, no. 4, pp. 619–627, Apr. 1991.

[29] P. Hoeher, *Kohärenter Empfang trelliscodierter PSK-Signale auf frequenzselektiven Mobilfunkkanälen – Entzerrung, Decodierung und Kanalparameterschätzung.* No. 147 in Fortschrittberichte VDI, VDI Verlag.

[30] P. Hoeher, "A statistical discrete-time model for the WSSUS multipath channel," *IEEE Transactions on Vehicular Technology,* vol. 41, no. 4, pp. 461–468, Nov. 1992.

[31] COST 207, "Digital land mobile radio communications," final report, Office for Official Publications of the European Communities, Brussels, Luxemburg, 1989.

[32] I. A. Gerson and M. A. Jasiuk, "Vector sum excited linear prediction (VSELP) speech coding at 8 kb/s," *Proceedings of the IEEE International Conference on Acoustics, Speech and Signal Processing,* pp. 461–464, Apr. 1990.

[33] D. Bodson, G. F. McClure, and S. R. McConoughey, eds., *Land-Mobile Communications Engineering*. New York: IEEE Press, 1984.

[34] CEPT/COST 207 WG1, "Proposal on channel transfer functions to be used in GSM tests late 1986," Tech. Rep. (86)51, COST 207 TD, Sept. 1986.

Volker Aue

Volker Aue was born in Lübeck, Germany, in 1969. After graduating from the Jungmannschule in Eckernförde with the degree "Abitur," he fulfilled his military service in the German Navy. There, he was involved in the detection and classification of radar signals. In October, 1989, he began studying Electrical Engineering at the Technische Universität Braunschweig in Germany. He also worked as a practical trainee at German Telekom and the Institute for Applied Microelectronics in Braunschweig.

Since August, 1992, he has been enrolled as a graduate student at Virginia Tech. He has taken several classes in communications and other related areas. In May, 1993, he joined the Mobile and Portable Radio Research Group (MPRG). His current research interests are equalization techniques and cyclostationarity. Volker Aue is member of the IEEE.